

Development

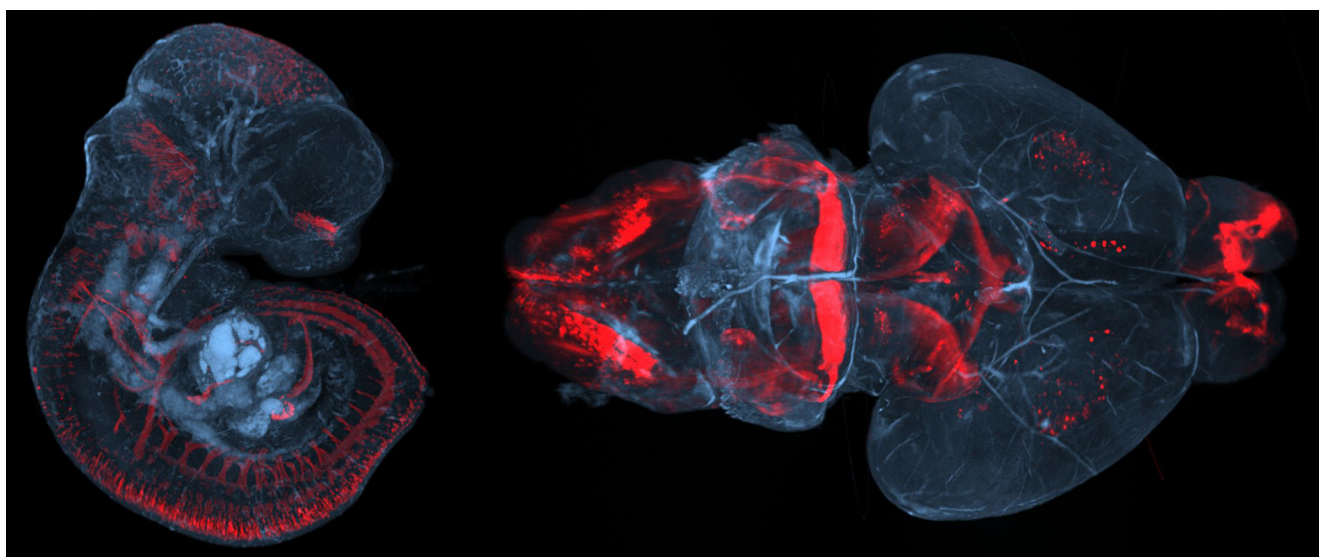
# Distinct Opsin 3 (*Opn3*) Expression in the Developing Nervous System during Mammalian Embryogenesis

Wayne I. L. Davies,<sup>1,\*</sup> Soufien Sghari,<sup>1,\*</sup> Brian A. Upton,<sup>2,3,4,\*</sup> Christoffer Nord,<sup>1</sup>  Max Hahn,<sup>1</sup> Ulf Ahlgren,<sup>1</sup> Richard A. Lang,<sup>3,4,5,6</sup> and  Lena Gunhaga<sup>1</sup>

<https://doi.org/10.1523/ENEURO.0141-21.2021>

<sup>1</sup>Umeå Centre for Molecular Medicine (UCMM), Umeå University, Umeå 901 87, Sweden, <sup>2</sup>Medical Scientist Training Program, University of Cincinnati, Cincinnati, OH 45229, <sup>3</sup>The Visual Systems Group, Abrahamson Pediatric Eye Institute, Cincinnati Children's Hospital Medical Center, Cincinnati, OH 45229, <sup>4</sup>Center for Chronobiology, Division of Pediatric Ophthalmology, Cincinnati Children's Hospital Medical Center, Cincinnati, OH 45229, <sup>5</sup>Division of Developmental Biology, Cincinnati Children's Hospital Medical Center, Cincinnati, OH 45229, and <sup>6</sup>Department of Ophthalmology, University of Cincinnati, College of Medicine, Cincinnati, OH 45221

## Visual Abstract



### Significance Statement

The expression of the mammalian Opsin 3 (*Opn3*) has only recently been characterized in adults, with no significant study during embryonic development. This study used an *Opn3*-eGFP mouse line to identify *Opn3*-related development of the central and peripheral nervous systems (CNS, PNS). 2D and 3D fluorescence imaging revealed cell body and axonal *Opn3*-eGFP expression, which indicated an early onset of *Opn3*-eGFP in cranial and spinal nerve ganglia, and sensory organs. Embryonic expression of *Opn3*-eGFP was also identified in the brainstem, cerebellum, hypothalamus and thalamus, whereas *Opn3*-eGFP expression in the cerebral cortex and associated limbic system regions were observed postnatally. The presence of *Opn3*, a short-wavelength-sensitive photopigment, in many brain regions during embryogenesis is of great interest when investigating autonomic and cognitive photo-dependent neural development.

Opsin 3 (*Opn3*) is highly expressed in the adult brain, however, information for spatial and temporal expression patterns during embryogenesis is significantly lacking. Here, an *Opn3*-eGFP reporter mouse line was used to monitor cell body expression and axonal projections during embryonic and early postnatal to adult stages. By applying 2D and 3D fluorescence imaging techniques, we have identified the onset of *Opn3* expression, which predominantly occurred during embryonic stages, in various structures during brain/head development. In addition, this study defines over twenty *Opn3*-eGFP-positive neural structures never reported before. *Opn3*-eGFP was first observed at E9.5 in neural regions, including the ganglia that will ultimately form the trigeminal, facial and vestibulocochlear cranial nerves (CNs). As development proceeds, expanded *Opn3*-eGFP expression coincided with the formation and maturation of critical components of the central and peripheral nervous systems (CNS, PNS), including various motor-sensory tracts, such as the dorsal column-medial lemniscus (DCML) sensory tract, and olfactory, acoustic, and optic tracts. The widespread, yet distinct, detection of *Opn3*-eGFP already at early embryonic stages suggests that *Opn3* might play important functional roles in the developing brain and spinal cord to regulate multiple motor and sensory circuitry systems, including proprioception, nociception, ocular movement, and olfaction, as well as memory, mood, and emotion. This study presents a crucial blueprint from which to investigate autonomic and cognitive opsin-dependent neural development and resultant behaviors under physiological and pathophysiological conditions.

**Key words:** brain; development; encephalopsin; nervous system; *Opn3*; OPT

## Introduction

Light detection (photoreception) and its related disorders are often focused on the visual system, where eyes and the specialized rod and cone photoreceptors they contain are crucial for forming images of the external world. However, it has become evident that there is a multiplicity of non-visual light detection processes, where specialized G-protein-coupled receptors (i.e., opsins) mediate both visual and non-visual photoreception. Briefly, the opsin protein moiety is covalently linked to a light-sensitive retinoid chromophore, which together form a photopigment (Yokoyama, 2000; Davies et al., 2012). In the presence of particular wavelengths of light, photopigments absorb the energy of a photon and, thereafter, activate functionally relevant phototransduction signaling

cascades (Shichida and Matsuyama, 2009; Lamb et al., 2016).

For many years, it was assumed that visual opsins in the rods and cones, and a subset of intrinsically photosensitive retinal ganglion cells (RGCs; see extended data for a list of abbreviations) were the only opsin-based photoreceptors present in mammals, all of which were restricted to the retina. However, ~20 years ago, so-called atypical or non-visual opsins, including Opsin 3 (*Opn3*, also known as encephalopsin or panopsin), *Opn4* (melanopsin), and *Opn5* (neuropsin), were identified in photoreceptors that were not thought to be involved in visual perception directly (Provencio et al., 1998; Blackshaw and Snyder, 1999; Tartelin et al., 2003b). Of these three opsins, melanopsin has been the most studied in terms of function in visual and non-visual light detection processes, where it has been shown to play a key role in circadian clock photoentrainment and pupillary constriction in mammals (Freedman et al., 1999; Lucas et al., 2003; Xue et al., 2011; Sghari et al., 2020). Other known non-visual effects of *Opn4* include DNA repair activation (Hirayama et al., 2009) and cell cycle regulation (Dekens et al., 2003). Nevertheless, in mammals, relatively little is known about non-visual light detection processes.

Consistent with reported light-regulated processes other than vision, the presence of atypical photopigments in multiple non-retinal adult tissues has been observed. For example, *Opn4* has been detected in melanocytes (Provencio et al., 1998), the iris (Xue et al., 2011; Sghari et al., 2020), cornea and associated trigeminal ganglia (Delwig et al., 2018), blood vessels and heart (Regard et al., 2008; Sikka et al., 2014), and *Opn5* being found in the eye, brain, testes, ear, and skin (Kojima et al., 2011; Buhr et al., 2015, 2019; Haltaufderhyde et al., 2015). The initial identification and expression of *Opn3* in the adult mouse brain, including regions like the cerebral cortex and cerebellum (Blackshaw and Snyder, 1999), have been verified and extended (Nissilä et al., 2012; Olinski et al., 2020b). Recent studies in the adult mammalian brain, especially that of rodents and some primates, indicate that *Opn3*

Received March 31, 2021; accepted August 11, 2021; First published August 20, 2021.

The authors declare no competing financial interests.

Author contributions: R.A.L. and L.G. designed research; W.I.L.D., S.S., B.A.U., C.N., and M.H. performed research; W.I.L.D., S.S., B.A.U., C.N., M.H., U.A., R.A.L., and L.G. analyzed data; W.I.L.D., S.S., and L.G. wrote the paper.

This research conducted in the Gunhaga laboratory was supported by the Swedish Research Council Grant 2017-01430, Insamlingsstiftelsen, Medical Faculty at Umeå University, and the Kempestiftelsen Grant SMK-1763. Work in the Lang laboratory was supported by National Institutes of Health Grants R01EY027077, R01EY027711, R01EY032029, and T32GM063483. Work in the Ahlgren laboratory was supported by the Swedish Research Council Grant 2017-01307 and Insamlingsstiftelsen, Medical Faculty at Umeå.

\*W.I.L.D., S.S., and B.A.U. contributed equally to this work.

Acknowledgements: We thank Maria Eriksson and Federico Morini, Umeå University, for technical advice related to 3D imaging protocols, and Paul Speeg, Cincinnati Children's Hospital, for mouse colony management. We also thank the following persons for kindly providing antibodies: Anna Överby Wernstedt (GFAP) and Helena Edlund (donkey anti-goat Alexa Fluor 488), both at Umeå University.

Correspondence should be addressed to Lena Gunhaga at [lena.gunhaga@umu.se](mailto:lena.gunhaga@umu.se).

<https://doi.org/10.1523/ENEURO.0141-21.2021>

Copyright © 2021 Davies et al.

This is an open-access article distributed under the terms of the Creative Commons Attribution 4.0 International license, which permits unrestricted use, distribution and reproduction in any medium provided that the original work is properly attributed.

exhibits a far wider expression profile (Nissilä et al., 2012; Olinski et al., 2020b), which suggests the potential for many unknown roles of light signaling in the brain and other organs. Notably in adult vertebrates, including higher mammals, *Opn3* is expressed in adipocytes and several tissues, such as, heart, intestine, kidneys, liver, ovaries, pancreas, placenta, pulmonary arteries, retina and associated eye structures, skeletal muscle, skin, testes, uterus, trachea, and lungs (Blackshaw and Snyder, 1999; Halford et al., 2001; Tarttelin et al., 2003a; Haltaufderhyde et al., 2015; Ortiz et al., 2018; Nayak et al., 2020; Olinski et al., 2020a; Yim et al., 2020; Wu et al., 2021). In addition, phylogenetic analyzes indicate that related orthologues of *Opn3* are present in all major vertebrate classes studied to date (Shichida and Matsuyama, 2009; Davies et al., 2015), suggesting a conserved function for this photopigment. The widespread adult expression pattern of these non-visual opsins suggests that light may play a broader functional role than previously thought. Whether non-visual opsins are also spatially and temporally expressed during embryonic stages, and if so, in which structures and when (i.e., the time of onset), have not been defined.

A sufficient number of photons is able to penetrate the skin, skull, soft tissues, including the mammalian brain itself, at both fetal and adult stages to activate photoreceptors (Dunn et al., 2015; Sun et al., 2016; Reid et al., 2017; Nayak et al., 2020; Zhang et al., 2020). Therefore, it is essential to determine whether *Opn3* might play a significant role in brain development and function. As such, the primary aims of this study were to use an *Opn3*-eGFP reporter mouse model to investigate the expression of *Opn3* throughout embryonic development, just after birth, as well as juvenile and adult stages. A combination of immunofluorescence techniques, including 3D imaging by optical projection tomography (OPT) was used.

This study provides a detailed appreciation of the early onset of *Opn3* at around embryonic day (E)9.5 and broad, yet distinct, expression of *Opn3* in the developing mammalian embryo. Specifically, numerous *Opn3*-eGFP-positive cranial ganglia, neural projections and nuclei were detected in the developing brain and spinal cord, which together identify key structures of major neural pathways and circuits. Collectively, these results form the basis of further investigations into how *Opn3*-dependent signaling might regulate the development of the nervous system and other key structures, which might prove significant in understanding the season-of-conception/birth dependent risk of developing several metabolic, neurologic and psychiatric diseases (Foster and Roenneberg, 2008).

## Materials and Methods

### Ethics statement

All animal procedures were performed in accordance with the Umeå University animal care committee's regulations.

### *Opn3*-eGFP reporter mice

A genetically-modified *Opn3*-eGFP (enhanced green fluorescent protein) reporter mouse strain (*Tg[Opn3-*

*EGFP]JY3Gsat*; MMRRRC/GENSAT stock number 030727-UCD, Mutant Mouse Resource and Research Centers, University of California, Davis, CA) was generated as detailed previously (Nayak et al., 2020). This reporter mouse strain contains an eGFP reporter gene inserted at the start of exon 1 of the coding sequence of *Opn3*, but downstream of the *Opn3* promoter. As such, eGFP expression was driven by the *Opn3* promoter and is stated as *Opn3*-eGFP herein. Animals were housed on a 12/12 h light/dark (LD) cycle in a temperature and humidity-controlled environment.

### Genotyping and PCR

Genotyping to confirm the presence of the *Opn3*-eGFP allele was performed using an oligonucleotide pair (forward primer, 5'-CAGAGCGTGAGATCCACCCTGTT-3'; reverse primer, 5'-TAGCGGCTGAAGCACTGCA-3') that generated an amplicon of 320 bp under the following PCR cycling conditions: an initial step of 94°C for 5 min, followed by 30 cycles of 94°C for 30 s, 56°C for 30 s, and 72°C for 30 s, and a final elongation step of 72°C for 7 min.

### Tissue preparation

Adult mice and pregnant females (one to five months) were perfused with fresh 4% paraformaldehyde (PFA) in 0.1 M phosphate buffer (PB; pH 7.4) that was filtered through a 0.2 µm syringe filter to remove particulates. Where stated, whole embryos, heads or brains from embryonic stages (E8.5, E9.5, E10.5, E13.5, E15.5, and E17.5), as well as from postnatal (P) stages 0.5, P10, and adults, were collected. At least three and up to five specimens of each time point were analyzed. In all cases, retrieved embryonic, postnatal or adult tissues were immersion-fixed in fresh filtered PFA (4%) at 4°C for 4 h to overnight (ON), before being stored in fresh 0.1 M PB at 4°C until further use.

### Immunohistochemistry

Gradual cryo-protection of whole embryos or selected tissues using 3.25–25% sucrose in PB at 4°C was performed, and thereafter embedded in NEG-50 (Cellab). Samples were stored at –80°C and cryo-sectioned with thickness at 20 µm (for E8.5–E10.5), 40 µm (for E13.5 to adult stages), or 10 µm (for E17.5 *Opn3*-eGFP/GFAP staining). For *Opn3*-eGFP reporter detection, immunohistochemistry was used by applying standard protocols (Wittmann et al., 2014) with a rabbit anti-GFP antibody (1:500 dilution; Thermo Fisher Scientific; #A11122) and an anti-rabbit IgG Cy3-conjugated secondary antibody (1:400 dilution; Jackson ImmunoResearch Europe; #111-165-003), or an anti-rabbit Alexa Fluor 488-conjugated secondary antibody (1:300, Jackson ImmunoResearch). For glial fibrillary acidic protein (GFAP) and *Opn3*-eGFP co-labeling, rabbit anti-GFAP (1:500 dilution; gift from Anna Överby Wernstedt, Umeå University) and goat anti-GFP (1:500 dilution; Thermo Fisher Scientific; #A600-101-215M) primary antibodies were used. Secondary antibodies used were; donkey anti-rabbit Alexa Fluor 594-conjugated (1:400



dilution; Thermo Fisher Scientific; #A21207) and donkey anti-goat Alexa Fluor 488-conjugated antibodies (1:400 dilution; Thermo Fisher Scientific; #A11055; gift from Helena Edlund, Umeå University), respectively. In all cases, 4',6-diamidino-2-phenylindole (DAPI; 1:400 dilution; Sigma-Aldrich) was included to counterstain nuclei. Slides were mounted with fluorescent mounting medium (Agilent Technologies). Immunohistochemistry sections were examined by fluorescence microscopy (Nikon Eclipse, E800; Nikon Instruments Europe), with images being captured using a Nikon DS-Ri1 digital camera and Nikon NIS-Elements F v4.6 software, before being processed with Photoshop Creative Cloud (CC) 2019 (Adobe).

## OPT

OPT scanning was performed on whole embryos at E10.5 and brains at P0.5. Sample preparation was performed essentially as previously described (Sharpe et al., 2002; Alanentalo et al., 2007; Eriksson et al., 2013), except for the addition of further freeze-thaw methanol steps to increase antibody permeabilization (for both samples at E10.5 and P0.5) and extended washing steps for P0.5 brain samples. For *Opn3*-eGFP detection, filtered (0.45  $\mu$ m) rabbit anti-GFP (1:500 dilution, Thermo Fisher Scientific; #A11122) and goat anti-rabbit IgG Cy3-conjugated secondary (1:400 dilution; Jackson ImmunoResearch Europe; #111-165-003) antibodies were used, incubating at RT for 48–72 h at each step. Specimens were briefly equilibrated and placed in filtered low melting point agarose (1.5%; SeaPlaque Agarose, Lonza) and mounted into positioned, before methanol treatment and clearing in benzyl alcohol and benzyl benzoate (ratio 1:2). Once adequately transparent, specimens were imaged using a Bioptics 3001 OPT scanner (SkyScan) using Texas Red (Ex/Em: 560  $\pm$  20 nm/610 nm LP; exposure time: 800 ms for E10.5 and 425 ms for P0.5) and FITC (Ex/Em: 425  $\pm$  20 nm/475 nm LP; exposure time: 450 ms for E10.5 and 200 ms for P0.5) filter sets to maximize *Opn3*-eGFP and anatomic (autofluorescence) signals, respectively. Computational postscanning processing were conducted as previously described (Cheddad et al., 2012). 3D tomographic reconstructions were performed using NRecon v1.6.9.18 software (SkyScan), with visualization and video production conducted by implementing Imaris 9.3.1 software (Bitplane).

## Results

In this study, the spatial and temporal expression of Opsin 3 (*Opn3*) was analyzed by examining an *Opn3* promoter-driven eGFP mouse line (*Opn3*-eGFP) with a main focus on embryonic central and peripheral nervous systems (CNS, PNS). The detection of *Opn3*-eGFP expression was optimized, by using a sequential combination of a primary GFP and a secondary Cy3 antibody, to amplify positive staining and reduce unspecific background labeling. To define both temporal and spatial expression of *Opn3*-eGFP, embryos and postnatal animals of several stages were analyzed using sections in coronal, transversal and sagittal orientations. The below presented *Opn3*-eGFP expression patterns were consistent observations

comprised from analyzing a minimum of three and up to five specimens of each time point.

### Early onset of *Opn3* expression in the developing nervous system

*Opn3*-eGFP expression was detected in the developing CNS and PNS at E9.5 (Extended Data Fig. 1-1), but not at E8.5 (data not shown). Cranial nerves (CNs) are part of the PNS that have both sensory and/or motor components that direct multiple sensory, motor and autonomic functions. The sensory part, including the ganglia, derives from cranial neural crest cells and ectodermal placode cells (Patthey and Gunhaga, 2011; Schlosser, 2014; Vermeiren et al., 2020). At E9.5, *Opn3*-eGFP expression was detected in cells of the early forming trigeminal ganglia and facio-acoustic ganglion complex, which will later give rise to the sensory branches of the trigeminal (CN V), facial (CN VII), and vestibulocochlear (CN VIII) CNs (Extended Data Fig. 1-1B,C,J,K). Furthermore, *Opn3*-eGFP-positive (*Opn3*-eGFP<sup>+</sup>) cells were observed in the basal plate of the neural tube along the anteroposterior axis of the future spinal cord (Extended Data Fig. 1-1A–D,L), as well as the second, third and fourth pharyngeal pouches (Extended Data Fig. 1-1A–C). Additional *Opn3*-eGFP<sup>+</sup> non-neural regions, which are not the subject of this study, included the gastrointestinal tract, the dorsal pancreatic bud and the developing heart (Extended Data Fig. 1-1A,B,D).

Scattered *Opn3*-eGFP expression was also observed in the olfactory placode (Extended Data Fig. 1-1E,F), the most ventral and dorsal regions of the diencephalic neuroepithelium (Extended Data Fig. 1-1G,H) and the dorsal outer lining of the mesencephalic neuroepithelium (Extended Data Fig. 1-1I). Thus, the onset of *Opn3* expression is  $\sim$ E9.5 in both the CNS and PNS.

### At E10.5, *Opn3*-eGFP is expressed in several motor-sensory related cells

At E10.5, *Opn3*-eGFP expression was detected in the expanding trigeminal ganglia near to the brainstem (Fig. 1A,C,H,I), in the facio-acoustic ganglion complex in close connection to the *Opn3*-eGFP negative (*Opn3*-eGFP<sup>-</sup>) otic vesicle (Fig. 1B,C,H,I), in the developing glossopharyngeal and inferior vagal ganglia, including peripheral projections of the vagal ganglia (Fig. 1B,C,H). Scattered *Opn3*-eGFP<sup>+</sup> cells were observed in the neuroepithelium of the brainstem at the level of the trigeminal ganglia, in contrast to the level of the facio-acoustic complex and otic vesicle, where *Opn3*-eGFP<sup>+</sup> cells were primarily located in the lateral lining of the brainstem neuroepithelium (Fig. 1H,I). Moreover, *Opn3*-eGFP was detected in the dorsal root ganglia, derived from neural crest cells, throughout the anteroposterior axis of the spinal cord (Fig. 1D,E,J). Several afferent processes of the dorsal root ganglia were also observed in the hindbrain region (Fig. 1D,E). Consistent with findings at E9.5 (Extended Data Fig. 1-1H–K), *Opn3*-eGFP<sup>+</sup> cells were observed along the basal plate of the caudal neural tube, including motor exit



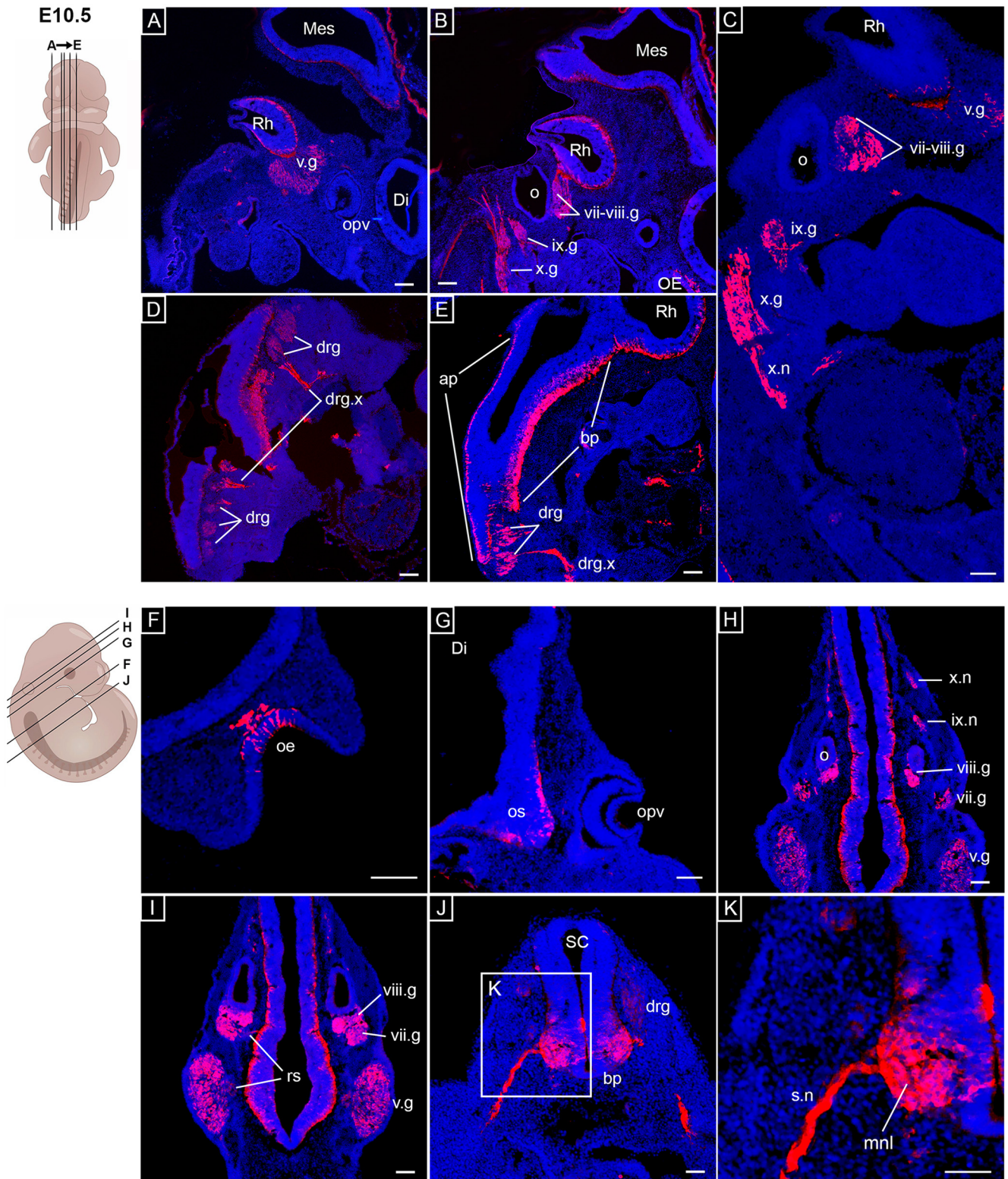


**Figure 1.** *Opn3*-eGFP immunodetection (red) at E10.5 in sagittal (**A–E**) and coronal (**F–K**) serial sections counterstained with DAPI (blue). On the left, schematics of E10.5 embryos including planes of sections shown in **A–K**. **A**, Di: diencephalic vesicle, Mes: mesencephalic vesicle, opv: optic vesicle, Rh: rhombencephalic vesicle, v.g: trigeminal ganglion. **B**, ix.g: glossopharyngeal ganglion, Mes: mesencephalic vesicle, o: otic vesicle, oe: olfactory epithelium, Rh: rhombencephalic vesicle, vii-viii.g: facio-acoustic ganglia, x.g: vagus ganglion. **A**, **B**, Parts of the amnion surrounding the embryo were digitally removed (raw data in Extended Data Fig. 1–3). **C**, ix.g: glossopharyngeal ganglion, o: otic vesicle, Rh: rhombencephalic vesicle, v.g: trigeminal ganglion, vii-viii.g: facio-acoustic ganglia, x.g: vagus ganglion, x.n: vagal nerve. **D**, drg: dorsal root ganglia, drg.x: dorsal root afferent processes. **E**, ap: alar plate, bp:

continued

basal plate, drg: dorsal root ganglia, drg.x: dorsal root afferent processes, Rh: rhombencephalic vesicle. **F**, oe: olfactory epithelium. **G**, Di: diencephalic vesicle, opv: optic vesicle, os: optic stalk. **H**, ix.n: glossopharyngeal nerve, o: otic vesicle, v.g: trigeminal ganglion, vii.g: geniculate ganglion, viii.g: vestibulocochlear ganglion, x.n: vagal nerve. **I**, rs: rootlets of the v/vii/viii.g, v.g: trigeminal ganglion, vii.g: geniculate ganglion, viii.g: vestibulocochlear ganglion. **J**, bp: basal plate, drg: dorsal root ganglion, SC: spinal cord. **K**, mnl: mantle layer, s.n: spinal nerves. Scale bars: 100  $\mu$ m. Extended Data Figures 1-1, 1-2 are supporting this figure.

points and related peripheral spinal nerve projections (Fig. 1J,K; Extended Data Fig. 1-2A-C).

By E10.5, the thickened olfactory placode has invaginated: at this stage, *Opn3*-eGFP expression was observed in both the olfactory epithelium and the nearby mesenchyme (Fig. 1F), which resembled patterns of postmitotic olfactory neurons (Miller et al., 2010; Panaliappan et al., 2018). Expression of *Opn3*-eGFP was also detected in the developing optic stalk; but at this stage, no expression was observed in the optic cup (Fig. 1G).

To obtain a global appreciation of *Opn3*-eGFP expression, with particular reference to the identified projections, 3D imaging by OPT was conducted, which verified the aforementioned *Opn3*-eGFP expression pattern noted in E10.5 sections. This included detection of *Opn3*-eGFP in different components of the PNS, such as nerves, ganglia, as well as sensory (otic) and somatosensory (skin, thorax, abdomen and limbs) projections toward their CNS targets, the hindbrain via the rootlets of cranial ganglia and the spinal cord via the dorsal root ganglia, respectively (Fig. 2; Movie 1). The uniform upregulation of *Opn3*-eGFP in the dorsal root ganglia along the anteroposterior axis of the embryo, as well as in projections emanating from dorsal root and cranial ganglion, and the olfactory placode were clearly visible (Fig. 2; Movie 1). Consistent with expression observed in E9.5 sections (Fig. 1), *Opn3*-eGFP was also observed in abdominal structures and the developing heart (Fig. 2; Movie 1).

### *Opn3*-eGFP detection in distinct ganglia and nerve fibers at E13.5

At E13.5, *Opn3*-eGFP was detected in many regions of the CNS, including cells of both the mantle and marginal layers of the spinal cord (Fig. 3A). The visualization of *Opn3*-eGFP labeled spinal motor neurons at E10.5, before sensory neurons located in the mantle layer, are consistent with the chronological differentiation of spinal motor neurons that precedes sensory neurons (Rodier, 1980). At the level of the medulla, *Opn3*-eGFP was detected in the spinal trigeminal nucleus, which receives information about deep/crude touch, pain and temperature from the face via all three branches of CN V (trigeminal), in addition to branches of CN VII (facial), CN IX (glossopharyngeal), and CN X (vagus; Fig. 3B,C). Consistently, *Opn3*-eGFP detection was also noted in trigeminal ganglia rootlets projecting to the principal sensory trigeminal nucleus (Fig. 3H), which receive information about discriminative sensation and light touch of the face, as well as conscious proprioception of the jaw via first order neurons of CN V.

*Opn3*-eGFP expression was also observed in the mesencephalic trigeminal nuclei (Fig. 3G), which are involved in both proprioception and motor functions of the jaw. Moreover, *Opn3*-eGFP was detected in the facial nerve (CN VII), including the genu of the facial nerve, which carries both sensory and autonomic fibers (Fig. 3G; Extended Data Fig. 1-2D-F). By this stage, *Opn3*-eGFP<sup>+</sup> vagal and glossopharyngeal ganglionic projections have

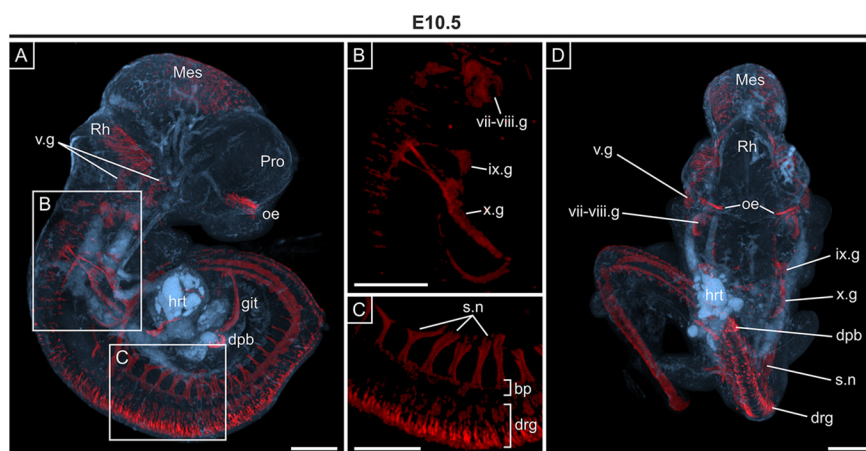
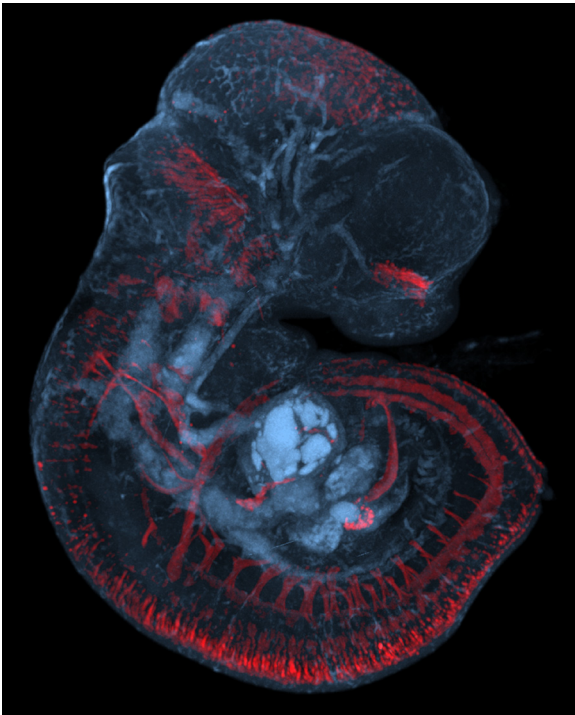


**Figure 2.** 3D OPT imaging of whole E10.5 embryo showing *Opn3*-eGFP immunodetection. **A**, Sagittal view showing detection of *Opn3*-eGFP (red) against a background of auto-fluorescing anatomical structures (blue). Developing ganglia that form the sensory branches of CNs V, CN VII, and CN VIII are shown in **B**, and spinal nerves highlighted in **C**, **D**. **D**, Dorsal view of embryo shown in **A**. bp: basal plate, dpb: dorsal pancreatic bud, drg: dorsal root ganglia, git: gastrointestinal tract, hrt: heart; ix.g: glossopharyngeal ganglion, Mes: mesencephalic vesicle, oe: olfactory epithelium, Pro: prosencephalic vesicle, Rh: rhombencephalic vesicle, s.n: spinal nerves, v.g: trigeminal ganglion, vii-viii.g: facio-acoustic ganglia (comprising the vii.g geniculate ganglion and viii.g: vestibulocochlear ganglion), x.g: vagus ganglion. Scale bars: 250  $\mu$ m.





**Movie 1.** Video of 3D imaging of a whole E10.5 embryo (along the *y*-axis) showing *Opn3*-eGFP immunodetection (red) against a background of auto-fluorescing anatomical structures (blue). [View online]

reached the posterolateral region of the medulla to form the solitary tract (Fig. 3C), which conveys afferent information from stretch receptors and chemoreceptors in the walls of the cardiovascular and respiratory systems, as well as the gastrointestinal tract. *Opn3*-eGFP was also detected in the parabrachial nuclei (Figs. 3F, 4C), which relay information from the solitary tract to the thalamus.

At E13.5, *Opn3*-eGFP was detected in both the hypoglossal nucleus and nucleus prepositus (also called nucleus prepositus hypoglossi; Fig. 3C,F), the latter of which plays an integral role in both vestibular and visual systems by integrating velocity and positional information for horizontal eye movements. *Opn3*-eGFP<sup>+</sup> vestibular fibers of the vestibulocochlear nerve (CN VIII) reach the medulla where they synapse with medullary vestibular nuclei, also detected as *Opn3*-eGFP<sup>+</sup> (Fig. 3C,E,F). Furthermore, *Opn3*-eGFP was detected in the medial longitudinal fasciculus (Fig. 3C), which form the ascending tract from the superior and medial vestibular nuclei. The medial longitudinal fasciculus terminates in the oculomotor-associated subnuclei that are located along the dorso-ventral and caudo-rostral regions of the tectum of the midbrain (Fig. 4A–C), as well as the abducens nucleus in the caudal portion of the pons (Fig. 3E). The cochlear nuclei, located in the junction of the pons and medulla where the auditory part of CN VIII synapses, were also identified as *Opn3*-eGFP<sup>+</sup> (Fig. 3D–F). In turn, the medullary cochlear nuclei send information to the superior olivary complex (Fig. 3D, E), the latter of which are a collection of nuclei important for ascending and descending auditory pathways.

In the cerebellum, *Opn3*-eGFP expression was detected in the external granular layer and deep cerebellar nuclei (Fig. 3D,G), as well as the superior cerebellar peduncle (Figs. 3F, 4A). This latter structure mainly consists of cerebellar efferent fibers that via the cerebello-rubral tract project to, among others, the contralateral red nucleus, which also was observed to be *Opn3*-eGFP<sup>+</sup> (Fig. 4B,C). Similarly, the tegmental decussations of ascending and descending fibers were *Opn3*-eGFP<sup>+</sup> (Fig. 4A,B).

At the level of the forebrain, *Opn3*-eGFP was detected in the subthalamic area and the dorsal thalamus (Fig. 4D–F), as were the projections of the cerebral peduncle to the dorsal thalamus and the medial forebrain bundles in the lateral hypothalamus (Fig. 4D,E). In addition, the dorso-medial and ventro-medial hypothalamic nuclei (Fig. 4D,E), which are related to the autonomic nervous system, and the stria medullaris (Fig. 4G), which is part of the epithalamus, were shown to express *Opn3*-eGFP. At this stage, the developing cerebral cortex did not express *Opn3*-eGFP (Fig. 4F). In both visual and olfactory systems, *Opn3*-eGFP was observed in RGCs, the optic nerve and tract (Fig. 4G,H), as well as the olfactory epithelium, nerve and bulb, and the vomeronasal organ and nerve (Fig. 4I).

#### Expanded *Opn3*-eGFP expression in sensory organs, tracts, and nuclei important for motor-sensory functions at E15.5

At E15.5, additional and expanded *Opn3*-eGFP<sup>+</sup> regions were observed (Figs. 5, 6). In the medulla, scattered cells expressing *Opn3*-eGFP were located in the medullary reticular nuclei (Fig. 5A,B), which are related to sleep behavior, and the magnocellular reticular nucleus (Fig. 5A, B), which project to the branchiomotor nuclei. Moreover, *Opn3*-eGFP expression was observed in the raphe obscurus, which are localized in the midline of the brainstem and involved with autonomic and motor activities (Fig. 5A, B). Close to the solitary tract, *Opn3*-eGFP was detected in the medullary ascending cuneate and gracile fasciculus (Fig. 5D). These fasciculi are part of the dorsal column-medial lemniscus (DCML) pathway, which transfer information about proprioception, exteroception and vibratory sensations from the trunk and extremities. This is consistent with findings at E10.5, where the posterior dorsal root ganglia, which are first order neurons in the DCML pathway, were confirmed to be *Opn3*-eGFP<sup>+</sup> (Fig. 1D,E,J). Furthermore, *Opn3*-eGFP expression was observed in the medial longitudinal fasciculus located in the lateral wall of the third ventricle (Fig. 5D,E), as well as the genu of the facial nerve (Fig. 5D,E) and the nucleus prepositus (Fig. 5F). The lateral vestibular nucleus in the upper medulla and the superior vestibular nucleus in the pons, which are both related to the vestibulo-ocular reflex when changing head and eye positions, were shown to express *Opn3*-eGFP (Fig. 5F,G).

In the pons, marked *Opn3*-eGFP expression was detected in the pontine nuclei (also called pontine gray; Fig. 5A,C) and the medial cerebellar peduncle (Fig. 5A,C), the latter of which conveys motor information regarding intended movements from the pontine nuclei to the contralateral cerebellum. At E15.5, a clear segregation of the



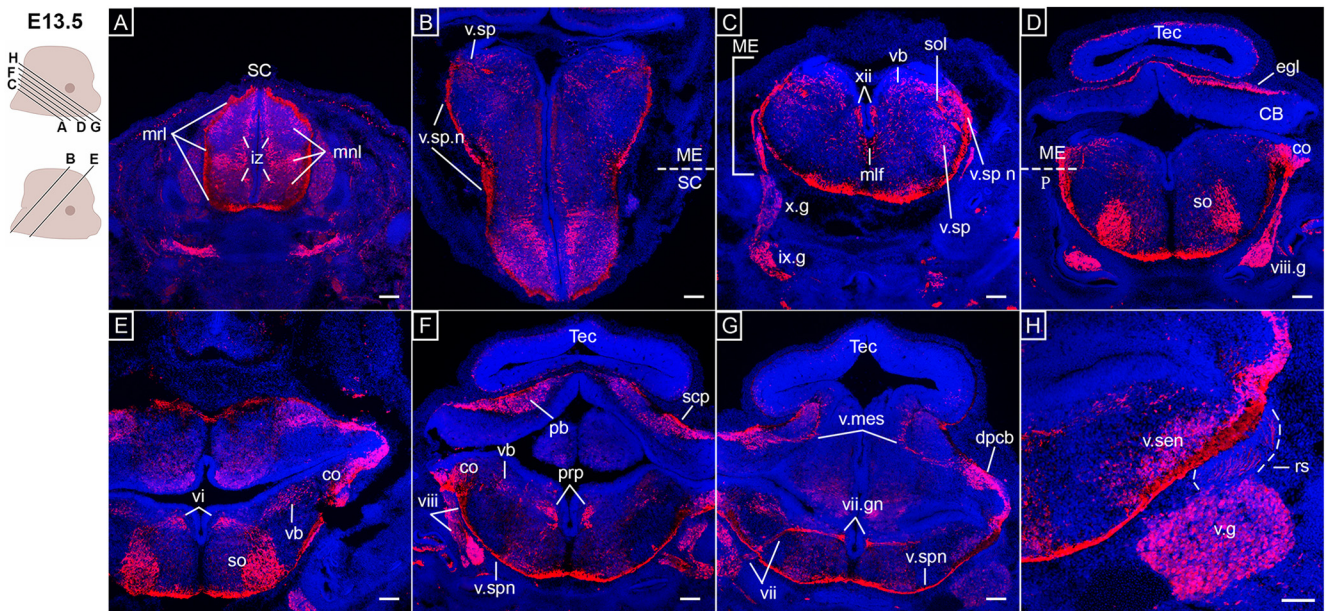


**Figure 3.** *Opn3*-eGFP immunodetection (red) at E13.5 in horizontal (**A**, **C**, **D**, **F–H**) and coronal (**B**, **E**) serial sections in caudo-rostral direction from the spinal cord to hindbrain areas counterstained with DAPI (blue). Left, Schematics of E13.5 embryonic heads including planes of sections shown in **A–H**. **A**, iz: intermediate zone, mnl: mantle layers, mrl: marginal layers, SC: spinal cord. **B**, ME: medulla, SC: spinal cord, v.sp n: spinal trigeminal nerve, v.sp: spinal trigeminal nucleus. **C**, ix.g: glossopharyngeal ganglion, ME: medulla, mlf: medial longitudinal fasciculus, sol: solitary tract, v.sp: spinal trigeminal nucleus, vb: vestibular nuclei, x.g: vagus ganglion, xii: hypoglossal nucleus. **D**, CB: cerebellum, co: cochlear nucleus, egl: external granular layer of cerebellum, ME: medulla; P: pons, so: superior olivary complex, Tec: tectum of midbrain, vii.g: geniculate (facial) ganglion. **E**, co: cochlear nucleus, so: superior olivary complex, vb: vestibular nuclei, vi: abducens nucleus. **F**, pb: parabrachial nuclei, scp: superior cerebellar peduncle, Tec: tectum of midbrain, v.sp.n: spinal trigeminal nerve, viii: vestibular nerve. **G**, dpcb: deep cerebellar nuclei, Tec: tectum of midbrain, v.mes: mesencephalic trigeminal nucleus, v.sp.n: spinal trigeminal nerve, vii.gn: genu of facial nerve, vii: sensory/parasympathetic facial nerve. **H**, rs: rootlets of the v.g, v.g: trigeminal ganglion, v.sen: sensory trigeminal nucleus. Scale bars: 100  $\mu$ m.

*Opn3*-eGFP<sup>+</sup> spinal, motor and sensory trigeminal nuclei were observed (Fig. 5D,F,G), as well as noted *Opn3*-eGFP expression in auditory structures such as the nucleus of the lateral lemniscus (Fig. 5D,G) and the brachium of the inferior colliculus (Fig. 6A). The pontine reticular nuclei (Fig. 5E–G) and the parabrachial nuclei (Fig. 6A), which relay solitary tract information to the forebrain, were detected as *Opn3*-eGFP<sup>+</sup>. In the cerebellum, *Opn3*-eGFP expression was observed in the dentate, fastigial, and interposed nuclei (Fig. 5H).

In the midbrain, *Opn3*-eGFP expression was observed in the reticular nuclei (Fig. 6A), the oculomotor-associated subnuclei (Fig. 6A; Extended Data Fig. 6–1) and the subthalamic area (Fig. 6F). *Opn3*-eGFP was also detected in the stria medullaris, containing afferent fibers from, among others, the *Opn3*-eGFP<sup>+</sup> septal nuclei, projecting to the habenular nuclei in the medial habenula (Fig. 6A,E,F). At this stage, *Opn3*-eGFP expression was identified in the decussation of the superior cerebellar peduncle and the ventral tegmental decussation (Fig. 6B,C). Consistently, the superior cerebellar peduncle consists of fibers carrying both cerebello-rubral and cerebello-thalamic tracts, here detected as *Opn3*-eGFP<sup>+</sup> (Fig. 6B–D), in which axons project from deep cerebellar nuclei (Fig. 3G) to the *Opn3*-eGFP<sup>+</sup> contralateral red nucleus (Fig. 6D) or the ventral lateral nucleus of the thalamus, respectively. Some

thalamic nuclei, known to act as relay stations between the midbrain and cortical areas, were also *Opn3*-eGFP<sup>+</sup>; these include the periventricular thalamus nucleus (Fig. 6B,E) that are associated with the limbic system, as well as the dorsal lateral geniculate nucleus (Fig. 6F), which is related to the visual pathway. Other central projections of the visual system were clearly labeled as *Opn3*-eGFP<sup>+</sup>, including the optic nerve, chiasm and tract (Fig. 6G,H), where visual information is transferred to the dorsal lateral geniculate nucleus. *Opn3*-eGFP expression was also observed in the olfactory sensory epithelium (Fig. 6H) and in parts of the auditory system, namely the pinna of the ear, vestibular nerve and geniculate ganglion (Fig. 6I). In addition, scattered *Opn3*-eGFP expression was also noted in the septal nuclei (Fig. 6F) and the paraventricular hypothalamic nucleus (Fig. 6G).

### Several *Opn3*-eGFP-positive forebrain nuclei are observed at E17.5

Additional *Opn3*-eGFP<sup>+</sup> structures were more clearly detected at E17.5 compared with earlier stages. Specifically, *Opn3*-eGFP expression was observed in the inferior colliculus (Fig. 7A), which receives auditory input from the superior olivary complex (Fig. 5A) via the lateral lemniscus (Fig. 7C, H), which was also observed to be *Opn3*-eGFP<sup>+</sup>. Moreover,



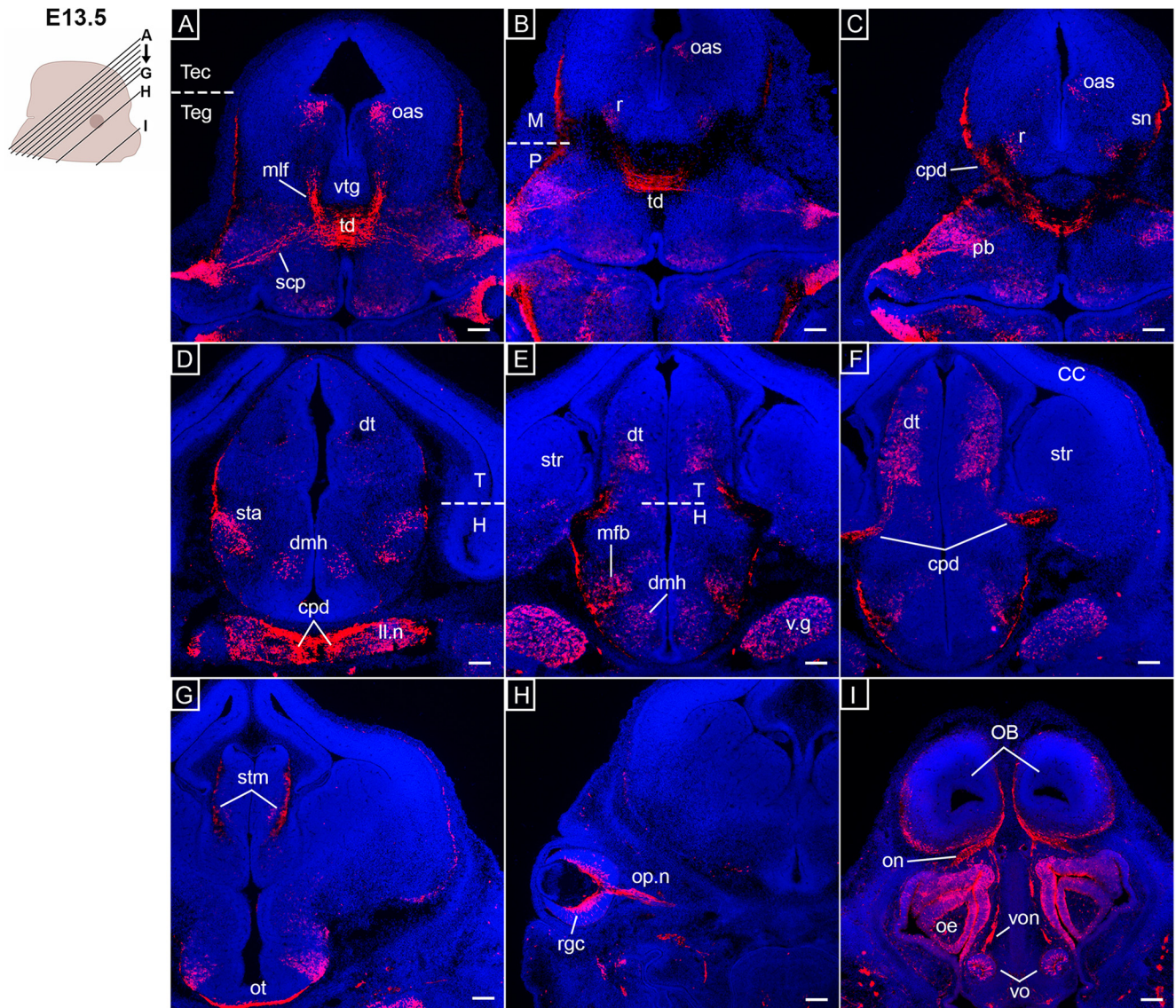


**Figure 4.** *Opn3*-eGFP immunodetection at E13.5 (red) in coronal serial sections caudo-rostral direction from midbrain to forebrain areas counterstained with DAPI (blue). On the left, a schematic of an E13.5 embryonic head including planes of sections shown in **A–I**. **A**, mlf: medial longitudinal fasciculus, oas: oculomotor associated subnuclei, scp: superior cerebellar peduncle, td: tegmental decussations, Tec: tectum of midbrain, Teg: midbrain and pontine tegmentum, vtg: ventral tegmentum. **B**, M: midbrain, oas: oculomotor associated subnuclei, P: pons, r: red nucleus, td: tegmental decussations. **C**, cpd: cerebral peduncle, oas: oculomotor associated subnuclei, pb: parabrachial nuclei, r: red nucleus, sn: substantia nigra. **D**, cpd: cerebral peduncle, dmh: dorsomedial hypothalamic nucleus, dt: dorsal thalamus, H: hypothalamus, ll.n: nucleus of lateral lemniscus, sta: subthalamic area, T: thalamus, v.g: trigeminal ganglion. **E**, dt: dorsal thalamus, H: hypothalamus, mfb: medial forebrain bundles, str: striatum, T: thalamus, dmh: dorsomedial hypothalamic nucleus. **F**, CC: cerebral cortex, cpd: cerebral peduncle, dt: dorsal thalamus, str: striatum. **G**, stm: stria medullaris, ot: optic tract. **H**, op.n: optic nerve, rgc: retinal ganglion cells. **I**, OB: olfactory bulb, oe: olfactory epithelia, on: olfactory nerve, vo: vomeronasal organ, von: vomeronasal nerve. Scale bars: 100  $\mu$ m.

the periaqueductal gray (Fig. 7B), which plays a critical role in the autonomic system, motivated behavior and pain modulation, was *Opn3*-eGFP<sup>+</sup>. In the cerebellum, the fastigial nucleus was *Opn3*-eGFP<sup>+</sup>, as was the uncinata fasciculus of the cerebellum (also known as the hooked bundle of Russell; Fig. 7B), which consists of fibers that descend to the superior cerebellar peduncle. In the midbrain, the cuneiform nucleus and midbrain reticular nuclei (Fig. 7C,E), both included in the midbrain reticular formation, were identified

as *Opn3*-eGFP<sup>+</sup>. Other *Opn3*-eGFP<sup>+</sup> midbrain-located nuclei comprised the deep nuclei of the superior colliculus (Fig. 7B,E) and the parafascicular nucleus (Fig. 7G,J), the latter of which is considered to be an essential thalamic structure in the feedback systems of basal ganglia-thalamo-cortical circuits involved in cognitive processes. At this stage, the rubro-spinal tract, which originates from the red nucleus and crosses the midline via the ventral tegmental decussation, were all detected by *Opn3*-eGFP (Fig. 7F), as was the



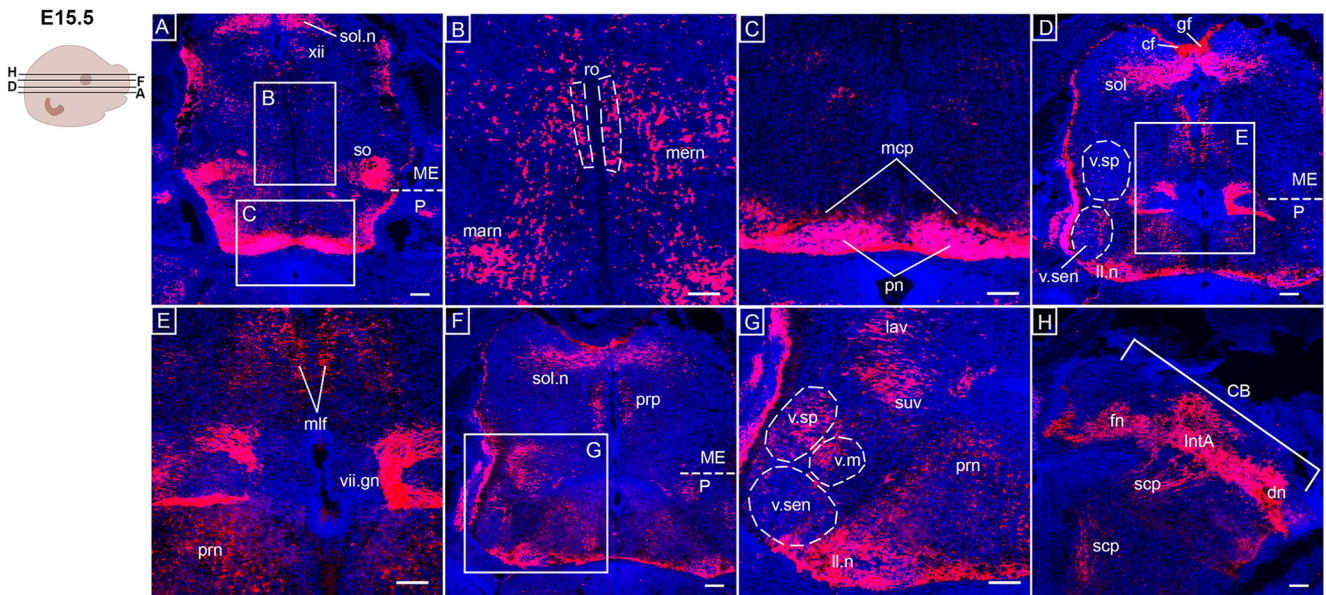


**Figure 5.** *Opn3*-eGFP immunodetection (red) at E15.5 in horizontal serial sections in caudo-rostral direction from the medulla to pons areas counterstained with DAPI (blue). On the left, a schematic of an E15.5 embryonic head including planes of sections shown in **A–H**. **A**, ME, medulla, P: pons, so: superior olivary complex, sol.n: solitary nucleus, xii: hypoglossal nucleus. **B**, marn: magnocellular reticular nucleus, mern: medullary reticular nuclei, ro: nucleus raphe obscurus. **C**, mcp: medial cerebellar peduncle, pn: pontine nuclei. **D**, cf: cuneate fasciculus, gf: gracile fasciculus, ll.n: nucleus of lateral lemniscus, ME: medulla, P: pons, sol: solitary tract, v.sen: sensory trigeminal nucleus, v.sp: spinal trigeminal nucleus. **E**, mlf: medial longitudinal fasciculus, prn: pontine reticular nuclei, vii.gn: genu of facial nerve. **F**, ME: medulla, P: pons, prp: nucleus prepositus, sol.n: solitary nucleus. **G**, lav: lateral vestibular nucleus, ll.n: nucleus of lateral lemniscus, prn: pontine reticular nuclei, suv: superior vestibular nucleus, v.m: motor trigeminal nucleus, v.sen: sensory trigeminal nucleus, v.sp: spinal trigeminal nucleus. **H**, CB: cerebellum, dn: dentate nucleus, fn: fastigial nucleus, IntA: interposed nucleus, scp: superior cerebellar peduncle. Scale bars: 100  $\mu$ m.

dorsal tegmental decussation (Fig. 7E). Furthermore, *Opn3*-eGFP expression was observed in the substantia nigra (Fig. 7G), a basal ganglia structure, and in the three white matter areas of the subthalamus, including the lenticular fasciculus, thalamic fasciculus and field H (Fig. 7I–K), in addition to the subthalamic nucleus (Fig. 7I).

At E17.5, *Opn3*-eGFP was detected in the pineal gland (Fig. 7J), an important structure well known to be involved in photoreception by producing melatonin during the dark phase of the sleep-wake cycle, as well as the ventro-medial thalamic nucleus (Fig. 7J,K), which projects pain-temperature information to the insular cortex. In the forebrain, *Opn3*-eGFP expression was observed in several hormone-releasing nuclei; namely the paraventricular and periventricular hypothalamic nuclei (Fig. 7L–N), and the medial preoptic nucleus (Fig. 7P), which all remained *Opn3*-eGFP<sup>+</sup> at postnatal/adult stages (Extended Data Fig. 7-1B,F,H). Other *Opn3*-eGFP<sup>+</sup> regions included the pyriform (olfactory) cortex (Fig. 7P); the subfornical organ (Fig. 7O), which is one of the circumventricular organs of the brain; and the nucleus accumbens (Fig. 7P), which is part of the reward and reinforcement systems. Moreover, scattered *Opn3*-eGFP expression was observed throughout the septum of the brain (Fig. 7O,P).

Studies of adult *Opn3::mCherry* reporter mice have reported that *Opn3* is expressed also in non-neuronal astrocytes (Olinski et al., 2020b). In mouse, the differentiation of astrocytes begins ~E17–E18 (Reemst et al., 2016; Matsue et al., 2018). To examine whether *Opn3* is

expressed in astrocytes at embryonic stages, double-immunohistochemistry of *Opn3*-eGFP and GFAP, a known astrocyte marker (Reemst et al., 2016), was performed at E17.5. At this stage, GFAP<sup>+</sup> astrocytes were identified in the hippocampus, in particular the dentate gyrus and the fimbria, and around the third ventricle at the level of the paraventricular hypothalamic nucleus, but GFAP was not co-expressed with *Opn3*-eGFP (Extended Data Fig. 7-1A–D). Moreover, GFAP<sup>+</sup> astrocytes were observed along the optic tract, in the glia limitans, the granular layer of olfactory bulb, septohippocampal nucleus, habenula, some regions of the stria medullaris and pyramidal tract, but again not co-expressed with *Opn3*-eGFP (Extended Data Fig. 7-1A,C,D; data not shown). Thus, these results indicate that *Opn3*-eGFP is not expressed in GFAP<sup>+</sup> astrocytes in the embryonic brain.

### Expanded *Opn3*-eGFP expression in the brain at postnatal and adult stages

Just after birth, at P0.5, an expansion of *Opn3*-eGFP expression was observed in the forebrain, including the cerebral cortex, with defined expression in the anterior cingulate cortex, involved in higher-level social functions (Fig. 8A,D), which was even more pronounced at P10 (Extended Data Fig. 8-1D). At P0.5, *Opn3*-eGFP expression was also noted in the striatum and in parts of the hippocampus, including the dentate gyrus (Fig. 8A,C). Moreover, *Opn3*-eGFP<sup>+</sup>-thalamic regions were identified,



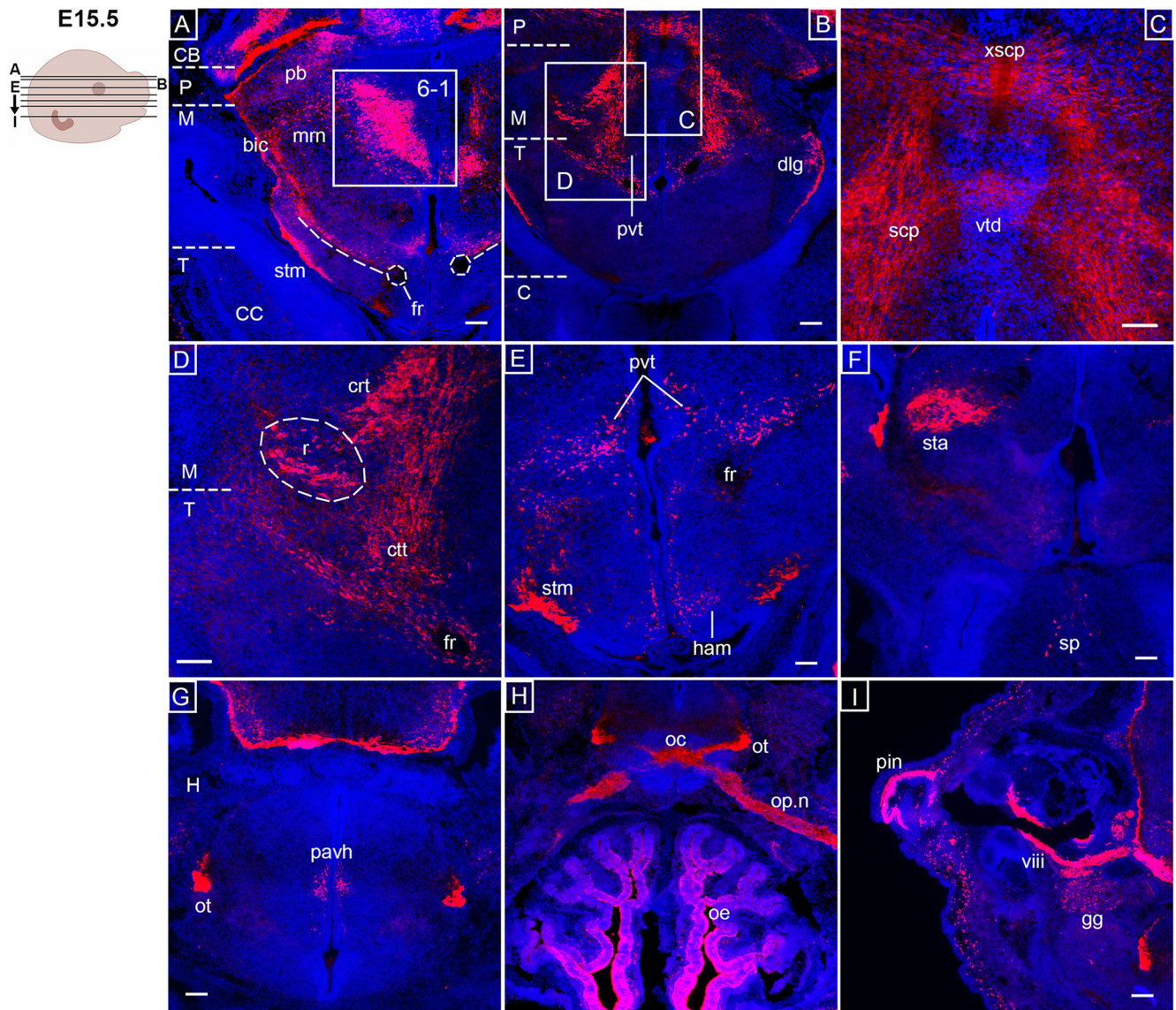


**Figure 6.** *Opn3*-eGFP immunodetection (red) at E15.5 in horizontal serial sections in caudo-rostral direction from the midbrain to forebrain areas counterstained with DAPI (blue). Left, Schematic of an E15.5 embryonic head including planes of sections shown in **A–I**. **A**, bic: brachium of inferior colliculus, CB: cerebellum, CC: cerebral cortex, fr: fasciculus retroflexus, M: midbrain, mrn: midbrain reticular nuclei, P: pons, pb: parabrachial nuclei, stm: stria medullaris, T: thalamus. The inserted box indicates area shown in Extended Data Figure 6-1. **B**, C: cerebrum, dlg: dorsal lateral geniculate nucleus, M: midbrain, P: pons, pvt: pvt: periventricular thalamic nucleus, T: thalamus. **C**, scp: superior cerebellar peduncle, vtd: ventral tegmental decussation, xscp: decussation of superior cerebellar peduncle. **D**, crt: cerebellar tract, ctt: cerebellothalamic tract, fr: fasciculus retroflexus, M: midbrain, r: red nucleus, T: thalamus. **E**, fr: fasciculus retroflexus, ham: medial habenula, pvt: periventricular thalamic nucleus, stm: stria medullaris. **F**, sp: septal nuclei, sta: subthalamic area. **G**, H: hypothalamus, ot: optic tract, pavh: paraventricular hypothalamus nucleus. **H**, oc: optic chiasm, oe: olfactory epithelium, op.n: optic nerve, ot: optic tract. **I**, gg: geniculate ganglion, pin: pinna of the ear, viii: vestibulocochlear nerve. Scale bars: 100  $\mu$ m.

including the posterior thalamus, lateral dorsal nucleus, as well as ventral posteromedial and lateral nuclei (Fig. 8A,B). Notably, the ventral posterolateral nucleus of the thalamus (Fig. 8A) receives information from, among others, the DCML pathway, which incorporated several *Opn3*-eGFP<sup>+</sup> structures detected at E15.5 (Fig. 5D). Also, *Opn3*-eGFP was detected in the dorsal lateral geniculate nucleus (Fig. 8B), which is a relay center for visual information from the optic nerve. At this stage, OPT imaging,

to appreciate the 3D perspective, clearly confirmed the expression of *Opn3*-eGFP in the medulla and pons, optic chiasm and tracts, dorsal lateral geniculate nuclei and areas of the primary visual cortex, as well as the olfactory bulb and several hypothalamic nuclei (Fig. 9; Movie 2).

Additional *Opn3*-eGFP<sup>+</sup> regions were identified at P10, namely the mammillary bodies and medial hypothalamic nuclei (Extended Data Fig. 8-1A), which are important for memory. Other parts of the limbic system that express



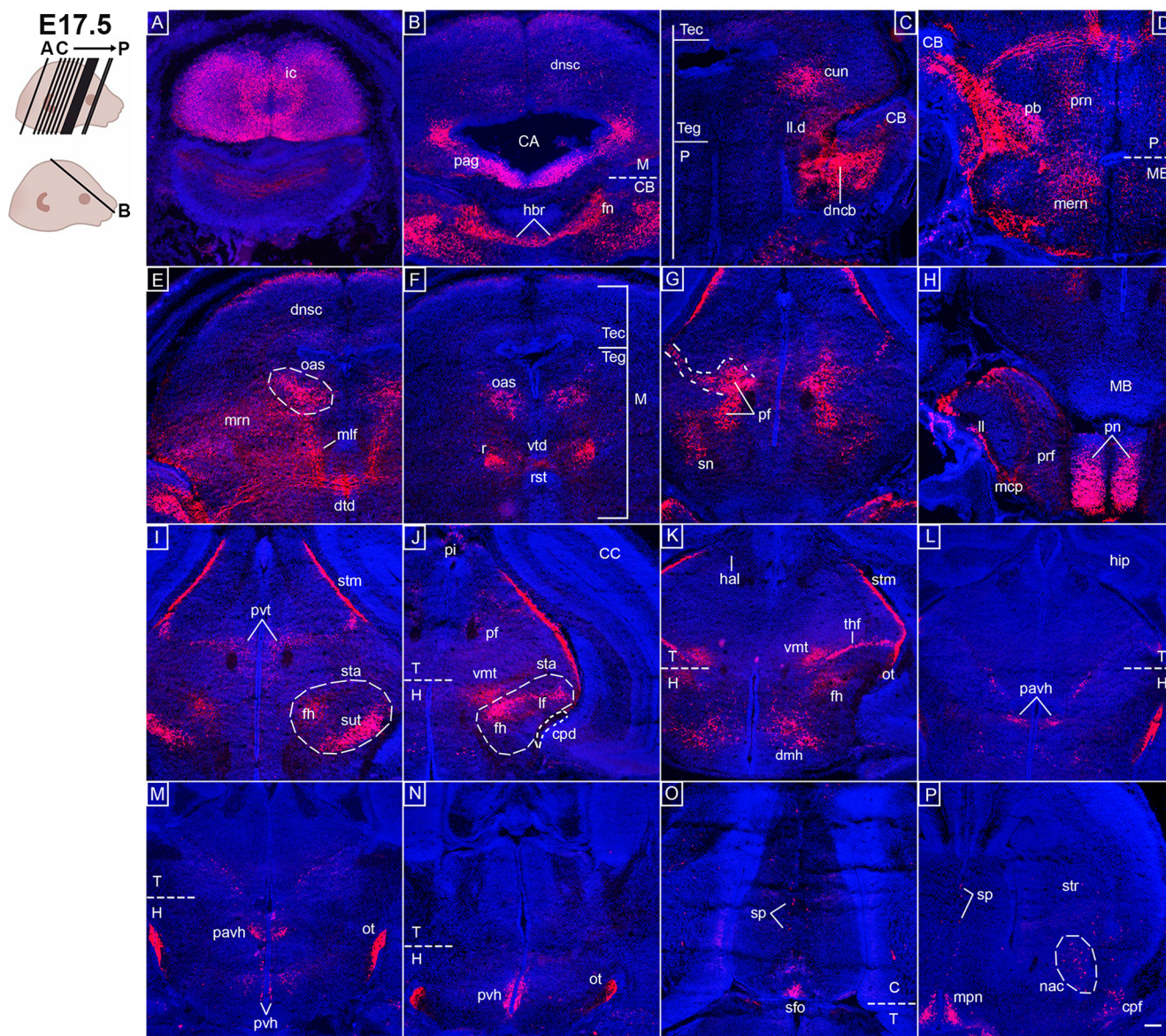


**Figure 7.** *Opn3*-eGFP immunodetection (red) at E17.5 in horizontal (**B**) and coronal (**A, C–P**) serial sections from the hindbrain to forebrain areas counterstained with DAPI (blue). Left, Schematic of E17.5 embryonic heads including planes of sections shown in **A–P**. **A**, ic: inferior colliculus. **B**, CA: cerebral aqueduct, CB: cerebellum, dnsc: deep nuclei of superior colliculus, fn: fastigial nucleus, hbr: hooked bundle of Russel, M: midbrain, pag: periaqueductal gray. **C**, CB: cerebellum, cun: cuneiform nucleus, dncb: deep nuclei of cerebellum, ll.d: dorsal component of lateral lemniscus, P: pons, Tec: tectum of midbrain, Teg: tegmentum of midbrain. **D**, CB: cerebellum, ME: medulla, mern: medullary reticular nuclei, P: pons, pb: parabrachial nuclei, prn: pontine reticular nuclei. **E**, dnsc: deep nuclei of superior colliculus dtd: dorsal tegmental decussation, mlf: medial longitudinal fasciculus, mrn: midbrain reticular nuclei, oas: oculomotor associated subnuclei. **F**, M: midbrain, oas: oculomotor associated subnuclei, r: red nucleus, rst: rubrospinal tract, Tec: tectum of midbrain, Teg: tegmentum of midbrain, vtd: ventral tegmental decussation. **G**, sn: substantia nigra, pf: parafascicular nucleus. **H**, ll: lateral lemniscus, MB: mamillary body, mcp: medial cerebellar peduncle, pn: pontine nuclei (gray), prf: pontine reticular nucleus. **I**, fh: field **H**, pvt: paraventricular thalamic nucleus, sta: subthalamic area, stm: stria medullaris, sut: subthalamic nucleus. **J**, CC: cerebral peduncle, cpd: cerebral peduncle, fh: field **H**, H: hypothalamus, lf: lenticular fasciculus, pf: parafascicular nucleus, π: pineal gland, sta: subthalamic area, T: thalamus, vmt: ventromedial thalamic nucleus. **K**, fh: field **H**, H: hypothalamus, hal: lateral habenula, ot: optic tract, stm: stria medullaris, T: thalamus, thf: thalamic fasciculus, dmh: dorsomedial hypothalamic nucleus, vmt: ventromedial thalamic nucleus. **L**, hip: hippocampus, H: hypothalamus, pavh: paraventricular hypothalamic nucleus, T: thalamus. **M**, H: hypothalamus, ot: optic tract, pavh: paraventricular hypothalamic nucleus, pvh: periventricular hypothalamic nucleus, T: thalamus. **N**, H: hypothalamus, ot: optic tract, pvh: periventricular hypothalamic nucleus, T: thalamus. **O**, C: cerebrum, sfo: subfornical organ, sp: septum of brain, T: thalamus. **P**, nac: nucleus accumbens, cpf: pyriform (olfactory) cortex, mprn: medial preoptic nucleus, sp: septum of brain, str: striatum. Scale bar: 100 μm. Extended Data Figure 7-1 is supporting this figure.



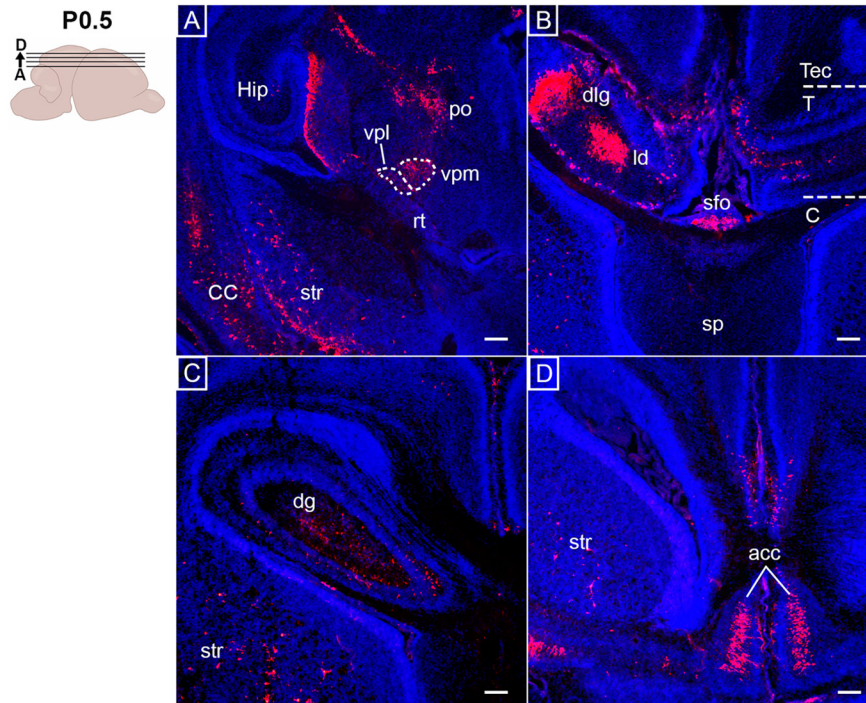


**Figure 8.** *Opn3*-eGFP immunodetection (red) at P0.5 in horizontal sections of forebrain areas counterstained with DAPI (blue). On the left, a schematic of a P0.5 brain including planes of sections shown in **A–D**. **A**, CC: cerebral cortex, Hip: hippocampus, p: posterior thalamus, rt: thalamic reticular nucleus, str: striatum, vpl: ventral posterolateral nucleus, vpm: ventral posteromedial nucleus. **B**, C: cerebrum, dlg: dorsal lateral geniculate nucleus, ld: lateral dorsal nucleus, sfo: subfornical organ, sp: septal nuclei, T: thalamus, Tec: tectum of midbrain. **C**, dg: dentate gyrus, str: striatum. **D**, acc: anterior cingulate cortex, str: striatum. Scale bars: 100  $\mu$ m. Extended Data Figure 8-1 is supporting this figure.

*Opn3*-eGFP included the anterior and posterior fibers of the fornix (Extended Data Fig. 8-1B,D,E), which connect the hippocampus with the forebrain. Furthermore, part of the cortico-striatal circuitry, between the anterior cingulate cortex and the striatum, which includes the reward system, were *Opn3*-eGFP<sup>+</sup> (Extended Data Fig. 8-1D). The posterior hypothalamus was also noted to express *Opn3*-eGFP (Extended Data Fig. 8-1B). The entorhinal cortex, important for spatial memory in relation to the hippocampus, was *Opn3*-eGFP<sup>+</sup>, as were the dentate gyrus and subiculum of the hippocampal formation (Extended Data Fig. 8-1C,D). In the thalamus, *Opn3*-eGFP expression was observed in the medial geniculate nucleus and the dorsal lateral geniculate nucleus (Extended Data Fig. 8-1C), which are related to auditory and visual pathways, respectively. The outer membrane, surrounding the brain also expressed *Opn3*-eGFP (Extended Data Fig. 8-1C).

During adulthood, *Opn3*-eGFP expression was identified in the perifornical lateral hypothalamic nuclei, which are related to respiratory control, and in  $\alpha$ -tanycytes that line the lateral walls of the third ventricle (Extended Data Fig. 8-1E). Furthermore, *Opn3*-eGFP was identified in the hormone-secreting supraoptic nucleus of the adult hypothalamus, including both the supraoptic nucleus proper and retro-chiasmatic supraoptic nucleus, and in the bed nucleus of the stria terminalis, which is a structure related to stress responses (Extended Data Fig. 8-1G,H). A few examples of areas that expressed *Opn3*-eGFP already at

embryonic stages that also were identified at early post-natal stages and in the adult brain, were the substantia nigra, the paraventricular and periventricular hypothalamic nuclei, the dorsal lateral geniculate nucleus, the septal nuclei, the dorsomedial hypothalamic nucleus and the preoptic area (Extended Data Fig. 8-1B–F).

## Discussion

Whereas most visual and non-visual opsins appear to be expressed in more or less restricted patterns, *Opn3* has been shown to be expressed in a broad range of multiple adult tissues (Blackshaw and Snyder, 1999; Nissilä et al., 2012; Olinski et al., 2020b). *Opn3* mRNA was first discovered in the cerebral cortex and cerebellum of the adult mouse brain (Blackshaw and Snyder, 1999), results that have been subsequently verified and expanded, most recently in studies using an *Opn3*::mCherry mouse model (Olinski et al., 2020b). Despite more detailed knowledge about the spatial expression of *Opn3* in the adult mouse brain, there is a significant lack of information concerning when and where in the nervous system *Opn3* is expressed during embryogenesis.

To address this issue, an *Opn3* promoter-driven eGFP mouse line was used to investigate *Opn3* expression in the developing nervous system with a focus on the brain/head region. A summary of *Opn3*-eGFP<sup>+</sup> key structures in relation to temporal onset of expression is outlined in Table 1. Notably, our study identified 25 new *Opn3*-



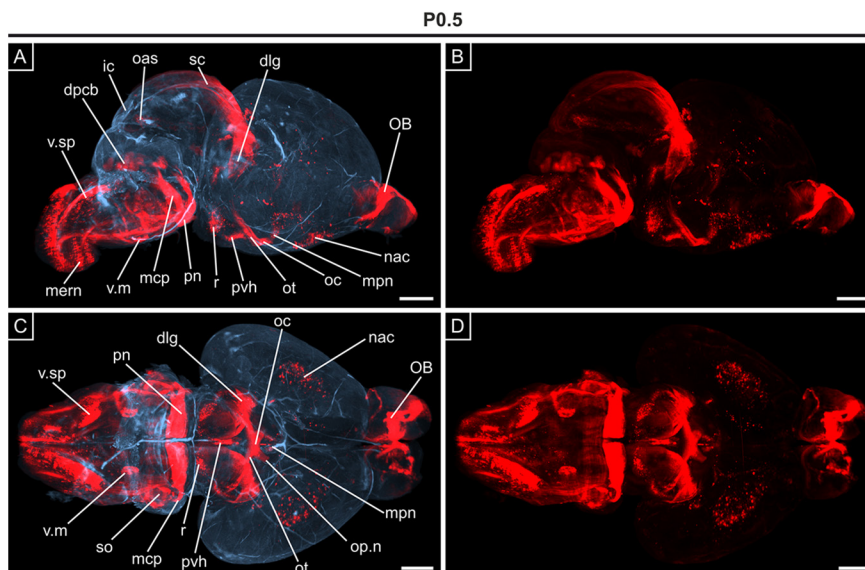


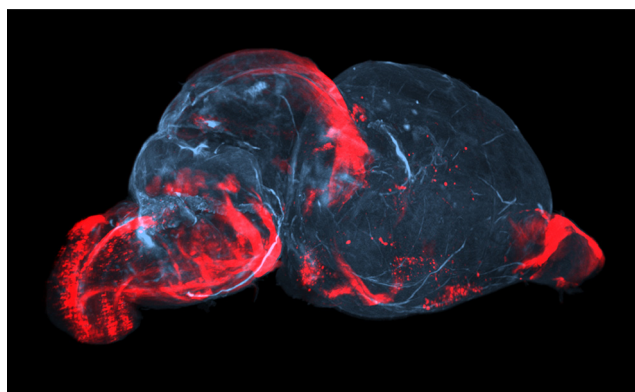
**Figure 9.** 3D OPT imaging of *Opn3*-eGFP immunodetection in the brain at P0.5. **A**, Sagittal view showing the presence of *Opn3*-eGFP (red) against a background of auto-fluorescing anatomic structures (blue). **B**, Repeat of **(A)** showing unmasked *Opn3*-eGFP (red) staining only. **C**, **D**, Ventral views of the brain shown in **A**, **B**, respectively. dlq: dorsal lateral geniculate nucleus, dpcb: deep nuclei of cerebellum, ic: inferior colliculus, mcp: medial cerebellar peduncle, mern: medullary reticular nuclei, mpn: medial preoptic nucleus, nac: nucleus accumbens, oas: oculomotor associated subnuclei, OB: olfactory bulb, oc: optic chiasm, op.n: optic nerve, ot: optic tract, pn: pontine nuclei (also pontine nuclei gray), pvh: periventricular hypothalamic nucleus, r: red nucleus, sc: superior colliculus, so: superior olivary complex, v.m: motor trigeminal nucleus, v.sp: spinal trigeminal nucleus. Scale bars: 1 mm.

eGFP<sup>+</sup> structures in the CNS and PNS, including sensory ganglions, the olfactory epithelium, vestibular nuclei and parafascicular nucleus, that have not been previously reported to express *Opn3* (Table 1). The analyzed *Opn3*-eGFP knock-in mouse line possesses two intact *Opn3* wild-type alleles that are consistent with an observed normal phenotype, which is in contrast to the recently developed *Opn3*::mCherry fusion protein mouse line (Olinski et al., 2020b). Being under the influence of the native *Opn3* promoter, both detected eGFP and *Opn3*::mCherry expression patterns appear to mirror the cellular expression profile of endogenous *Opn3* from earlier reports. Moreover, *Opn3*-eGFP cellular expression in the adult brain, as

characterized by this current study, mirrors that shown for *Opn3*::mCherry (Olinski et al., 2020a), which implicates that both *Opn3* reporter mice are accurately detecting *Opn3*-positive cells. As eGFP is a cytoplasmic protein, the reporter molecule is free to diffuse throughout the cell. As such, not only cell bodies, but also axonal projections are readily visible in the *Opn3*-eGFP reporter mouse line used here, which is greatly informative when analyzing anatomical-functional relationships.

In this study, evidence is provided that *Opn3* is expressed during most of embryonic development, and *Opn3*-eGFP was detected already at E9.5, much earlier than previously reported, in structures within the CNS and PNS. This timeline of expression indicates that *Opn3* may be the earliest of the opsin family of genes to be expressed in mammalian development. At E9.5–E10.5, *Opn3*-eGFP expression was detected in most, if not all, spinal nerves, their associated dorsal root ganglia, as well as several sensory ganglia, all of which are part of the PNS. The sensory ganglia form first order sensory neurons projecting to somatic tissues via ascending sensory tracts to brainstem and forebrain regions, while the spinal cord motor neurons form first order motor neurons connected directly to muscles (Chen et al., 2017). Results presented here show *Opn3*-eGFP expression in motor neurons and spinal nerves at E10.5, before observed *Opn3*-eGFP expression in sensory neurons at E13.5, which are in agreement with the temporal differentiation of first order spinal motor neurons before sensory neurons (Rodier, 1980).

Following embryonic growth, the temporal onset of *Opn3*-eGFP expression correlated with the development



**Movie 2.** Video of 3D imaging of a P0.5 brain (along the x-axis) showing *Opn3*-eGFP immunodetection (red) against a background of auto-fluorescing anatomical structures (blue). [View online]

**Table 1. A Summary outlining the onset of *Opn3*-eGFP expression in various structures of the CNS and PNS, indicating novel *Opn3*-eGFP<sup>+</sup> structures identified in this study (\*)**

PNS and sensory organs	CNS	Age
Trigeminal ganglion •	Neural tube	E9.5
Facio-acoustic complex ganglion •	Brain	E9.5
	vesicles	
Olfactory placode	Dorsal outer cells of mesencephalon	E10.5
Dorsal root ganglion	Motor neurons	
Inferior vagus ganglion •	Brain	E10.5
Glossopharyngeal ganglion •		
Migratory olfactory neurons	vesicles	E13.5
Retinal ganglion cells	Spinal cord	
Optic nerve	Dorsal, lateral and ventral mantle and marginal layers	E13.5
Olfactory epithelium •	Hindbrain	
Olfactory nerve •	Hindbrain	E13.5
Vomeranase organ •		
Vomeranase nerve •	Principal sensory trigeminal nucleus •	E13.5
	Mesencephalic trigeminal nucleus •	
	Genu of facial nerve •	E13.5
	Solitary tract	
	Parabrachial nuclei •	E13.5
	Hypoglossal nucleus •	
	Nucleus prepositus •	E13.5
	Vestibular nuclei •	
	Medial longitudinal fasciculus	E13.5
	Abducens nucleus •	
	Cochlear nuclei •	E13.5
	Superior olivary complex	
	External granular layers of cerebellum	E13.5
	Deep cerebellar nuclei	
	Superior cerebellar peduncle	E13.5
	Midbrain	
	Red nucleus	E13.5
	Oculomotor associated sub nuclei •	
	Tegmental fibres	E13.5
	Forebrain	
	Subthalamic area	E13.5
	Dorsal thalamus	
	Dorsal medial hypothalamic nucleus	E13.5
	Stria medullaris	
	Optic tract	E13.5
	Olfactory bulb	
Pinna of the ear	Hindbrain	E15.5
	Medullary reticular nuclei	E15.5
	Magnocellular reticular nucleus	
	Raphe obscurus •	E15.5
	Cuneate and gracile nuclei •	
	Pontine nuclei	E15.5
	Medial cerebellar peduncle •	
	Motor trigeminal nucleus	E15.5
	Nucleus of lateral lemniscus	
	Brachium of inferior colliculus	E15.5
	Midbrain	
	Midbrain reticular nuclei	E15.5
	Inferior colliculus	
	Brachium of inferior colliculus	E15.5
	Forebrain	
	Periventricular thalamic nucleus	E15.5
	Dorsal lateral geniculate nucleus	
	Septal nuclei •	E15.5
	Paraventricular hypothalamic nucleus	
Cerebellum	Uncinate fasciculus of cerebellum	E17.5
Midbrain	Periaqueductal gray •	E17.5
	Cuneiform nucleus	
	Rubrospinal tract	E17.5
	Substantia nigra	
Epithalamus	Pineal gland	E17.5

(Continued)

**Table 1.: Continued**

PNS and sensory organs	CNS	Age
	Thalamus	E17.5
	Parafascicular nucleus •	
	Ventromedial thalamic nucleus	E17.5
	Subthalamus	
	Subthalamic nucleus	E17.5
	Hypothalamus	
	Periventricular hypothalamic nucleus	E17.5
	Medial hypothalamic nucleus	
	Cerebrum	E17.5
	Subfornical organ	
	Nucleus accumbens	E17.5
	Pyrimiform cortex	
	Thalamus	P0.5
	Posterior thalamus	P0.5
	Lateral dorsal nucleus	
	Ventral posteromedial nucleus	P0.5
	Ventral posterolateral nucleus	
	Subpallium	P0.5
	Dentate gyrus of hippocampus	
	Pallium	P0.5
	Anterior cingulate cortex	
	Frontal cortex	P10
	Hypothalamus	
	Mammillary nuclei	P10
	Posterior nucleus	
	Subpallium	P10
	Fornix	
	Subiculum	P10
	Corticostrial circuitry	
	Meninges	Adult
	Outer membrane	
	Hypothalamus	Adult
	Perifornical nuclei	
	Tanycytes	Adult
	Supraoptic nucleus	
	Bed nucleus of stria terminalis	Adult

of individual neural structures in specific pathways and circuits (Chen et al., 2017), which indicates a potential role for *Opn3* in early neural development and subsequent maturation. Among the different sensory systems, the olfactory-associated pathway is the first to express *Opn3*-eGFP, with expression observed in the olfactory placode at E9.5, followed by postmitotic migratory neurons at E10.5, the nerve and bulb at E13.5 and the olfactory cortex at E17.5. *Opn3* is also expressed in the visual system, where *Opn3*-eGFP was evident in the optic stalk at E10.5, as well as RGCs at E13.5, including their *Opn3*-eGFP<sup>+</sup> axons in the optic nerve. Consistently, a previous study demonstrated by RT-PCR that *Opn3* is expressed at E10.5 during ocular development in mouse (Tartelin et al., 2003a). The optic nerves send central projections to the dorsal lateral geniculate nucleus of the thalamus, in this study detected by *Opn3*-eGFP from E15.5, and to the primary visual cortex, shown to express *Opn3* at adulthood (Olinski et al., 2020b). From E13.5 to adult stages, *Opn3*-eGFP expression expands throughout the spinal cord, brainstem and forebrain. Ventral, intermediate and dorsal gray matters in the spinal cord were identified as *Opn3*<sup>+</sup> regions that form motor, autonomic and sensory spinal cord components. Moreover, the onset of *Opn3*-eGFP in the hypothalamic paraventricular nucleus ~E15.5, was followed by the detection of *Opn3*-eGFP in the periventricular nucleus, dorsomedial hypothalamic nucleus and the medial preoptic nucleus, all of which were obvious at E17.5. Moreover, *Opn3*-eGFP expression was noted in the basal ganglia at E15.5, which connects to multiple thalamic nuclei with clear expression at E17.5, including the parafascicular



nucleus, a part of the medial and intralaminar nuclei that is hypothesized to play a critical role in the sensorimotor process of attentional orienting and behavioral flexibility (Brown et al., 2010; Yamanaka et al., 2018). Other *Opn3*-eGFP<sup>+</sup> subthalamic structures that are related to the basal ganglia, and involved in modulated motor control, include the white and gray matters of the fields of Forel, a structure implicated in epilepsy, movement and behavioral disorders (Neudorfer and Maarouf, 2018), as well as the subthalamic nucleus. All of the above are examples of that *Opn3*-eGFP onset of expression follows the individual developmental maturation of these neural structures.

In brief, thalamic nuclei connect various CNS structures with the cerebral cortex. Interestingly, no *Opn3*-eGFP expression was detected in association with the thalamic nuclei until after birth at P0.5. Consistently, the cerebral cortex was also *Opn3*-negative before birth, with cortical *Opn3*-eGFP expression coinciding with the onset of expression in the thalamic lateral dorsal, ventral posteromedial and ventral posterolateral nuclei at P0.5. In the cerebral cortex, observed *Opn3*-eGFP<sup>+</sup> areas included the pyriform cortex (~E17.5), cingulate cortex and archicortex (the hippocampus and associated structures; ~P0.5), and the entorhinal cortex (~P10). In subcortical areas, *Opn3*-eGFP was detected in the septal nuclei and nucleus accumbens at ~E17.5. Other extra-cortical structures that form part of limbic system were also shown to express *Opn3*-eGFP, namely the hypothalamic mammillary bodies (~P10) and the ventral medial thalamic nucleus (~E17.5). Consistently, previous reports have shown that *Opn3* is detectable in the cingulate, insula and frontal cortical regions of the adult brain, mainly in layer V pyramidal neurons that are characterized mainly by their cortico-striatal projections (Blackshaw and Snyder, 1999; Olinski et al., 2020b). These latter structures are required for appropriate goal-directed behaviors, including motivation and cognitive processes that mediate appropriate actions to obtain a specific outcome (Gerfen et al., 2013; Haber, 2016). As such, the presence of *Opn3*-eGFP in limbic-associated regions suggests potential (photoreceptive) roles in motivation, emotion, learning and memory.

The absence of *Opn3*-eGFP expression is also of functional significance and importance. In particular, *Opn3*-eGFP was not detected in the cerebral crus that carry cortico-spinal, cortico-bulbar (brainstem), and cortico-pontine tracts. As such, these data suggest that cortical nuclei expressing *Opn3*-eGFP in the frontal cortex are part of the inter-telencephalic cortico-striatal circuitry, with the exclusion of pyramidal neural network. Thus, *Opn3* is most likely restricted to either the premotor and/or supplementary motor areas in the frontal cortex, where all cortico-striatal connections are required before facilitating movement.

By using *Opn3*-eGFP as a cytoplasmic reporter, it was possible to track and trace neuronal cell bodies and their axonal projections for all *Opn3*<sup>+</sup> cell types. As a result, *Opn3*-eGFP was detected in the dorsal, lateral and ventral marginal layers that form the nerves of the second order DCML sensory tract, including both gracile and cuneate

fasciculi, as well as spinothalamic, spinocerebellar, spino-tectal, spino-reticular, and spino-vestibular tracts. These data suggest a possible involvement of *Opn3* in modulating sensory information pertaining to proprioception and fine touch. Also, from E13.5, the presence of *Opn3*-eGFP in higher CNS structures located in the brainstem identified second order ascending (brainstem to forebrain) and descending (brainstem to spinal cord) tracts. These include: (1) the trigeminal lemniscus (carrying sensory information from sensory and spinal trigeminal nuclei to the ventral posteromedial nucleus of the thalamus); (2) the vestibulo-ocular tract (from medullary vestibular nuclei to the oculomotor associated subnuclei via the medial longitudinal fasciculus); and (3) tracts of the auditory system (from the cochlear nucleus to the superior olivary complex, followed by the lateral lemniscus, then the inferior colliculus, and finally the medial geniculate nucleus). Further tracts identified by *Opn3*-eGFP were: (4) the solitary-parabrachial tract (carrying sensory information from CN VII, CN IX, and CN X to the solitary nucleus and parabrachial nuclei); (5) the cerebellar peduncles [including the superior (deep cerebellar nuclei projections), medial (pontine nuclei projections), and inferior (spino-cerebellar tract)]; and (6) the cerebral peduncle that mainly carries sensory input to the forebrain. Together these observations emphasize that studies of *Opn3*-eGFP expression can be used to follow projections for various neural systems and that *Opn3* appears to play a role in the development of multiple sensory pathways.

Given that *Opn3* has been shown to functionally form a short-wavelength-sensitive photopigment, with a spectral peak of absorbance in the blue range (Sugihara et al., 2016), the widespread expression pattern of *Opn3* during embryogenesis and well into adulthood suggests that mammalian photoreception could be far more complex than previously understood. Furthermore, the mechanisms by which they transduce photic signals to control physiology, or are affected in pathophysiological conditions, are either poorly understood or unknown. Thus, it remains to be shown that physiological levels of light can activate *Opn3* in the mammalian brain. Mental health disorders, such as depression, seasonal affective disorder (SAD; via a Pro10Leu mutation in a related opsin gene, *OPN4*; Roecklein et al., 2009), anxiety, schizophrenia, bipolar disorder, Alzheimer's disease, and other forms of dementia are associated with photosensory disruption (Foster et al., 2013). Moreover, there is a season-of-conception/birth dependent risk to develop these disorders (Foster and Roenneberg, 2008), which further indicates that light may play a crucial role for establishing optimal neural connections. Recently, studies have begun to uncover the neural basis linking light detection and depression/relaxation. One such study identified a suprachiasmatic nucleus-independent pathway, where photosensitive RGCs project to the perihabenular region of the thalamus, a retina-brain circuit that is strongly implicated in modulating mood (Fernandez et al., 2018). Given the detection of *Opn3*-eGFP in both the retina and thalamus, it is possible that dysfunction of *Opn3*-dependent photosensory systems may also be involved in mood regulation. What functional disturbances a modulation of *Opn3* might cause in regions of the

developing embryo, as well as adults, remains to be determined. Nonetheless, the temporal and spatial control of widespread, yet distinct, *Opn3* expression raises the possibility that this photopigment and/or other components of the *Opn3*-dependent phototransduction cascade play important roles in critical neuronal circuits. In conclusion, this study presents a crucial blueprint from which to investigate autonomic and cognitive opsin-dependent neural development and resultant behaviors under physiological and pathophysiological conditions.

## References

- Alanentalo T, Asayesh A, Morrison H, Lorén CE, Holmberg D, Sharpe J, Ahlgren U (2007) Tomographic molecular imaging and 3D quantification within adult mouse organs. *Nat Methods* 4:31–33.
- Blackshaw S, Snyder SH (1999) Encephalopsin: a novel mammalian extraretinal opsin discretely localized in the brain. *J Neurosci* 19:3681–3690.
- Brown HD, Baker PM, Ragozzino ME (2010) The parafascicular thalamic nucleus concomitantly influences behavioral flexibility and dorsomedial striatal acetylcholine output in rats. *J Neurosci* 30:14390–14398.
- Buhr ED, Yue WW, Ren X, Jiang Z, Liao HW, Mei X, Vemarraju S, Nguyen MT, Reed RR, Lang RA, Yau KW, Van Gelder RN (2015) Neuropsin (OPN5)-mediated photoentrainment of local circadian oscillators in mammalian retina and cornea. *Proc Natl Acad Sci USA* 112:13093–13098.
- Buhr ED, Vemarraju S, Diaz N, Lang RA, Van Gelder RN (2019) Neuropsin (OPN5) mediates local light-dependent induction of circadian clock genes and circadian photoentrainment in exposed murine skin. *Curr Biol* 29:3478–3487.e4.
- Cheddad A, Svensson C, Sharpe J, Georgsson F, Ahlgren U (2012) Image processing assisted algorithms for optical projection tomography. *IEEE Trans Med Imaging* 31:1–15.
- Chen VS, Morrison JP, Southwell MF, Foley JF, Bolon B, Elmore SA (2017) Histology atlas of the developing prenatal and postnatal mouse central nervous system, with emphasis on prenatal days E7.5 to E18.5. *Toxicol Pathol* 45:705–744.
- Davies WI, Collin SP, Hunt DM (2012) Molecular ecology and adaptation of visual photopigments in craniates. *Mol Ecol* 21:3121–3158.
- Davies WI, Tamai TK, Zheng L, Fu JK, Rihel J, Foster RG, Whitmore D, Hankins MW (2015) An extended family of novel vertebrate photopigments is widely expressed and displays a diversity of function. *Genome Res* 25:1666–1679.
- Dekens MP, Santoriello C, Vallone D, Grassi G, Whitmore D, Foulkes NS (2003) Light regulates the cell cycle in zebrafish. *Curr Biol* 13:2051–2057.
- Delwig A, Chaney SY, Bertke AS, Verweij J, Quirce S, Larsen DD, Yang C, Buhr E, VAN Gelder R, Gallar J, Margolis T, Copenhagen DR (2018) Melanopsin expression in the cornea. *Vis Neurosci* 35:E004.
- Dunn K, Reissland N, Reid VM (2015) The functional foetal brain: a systematic preview of methodological factors in reporting foetal visual and auditory capacity. *Dev Cogn Neurosci* 13:43–52.
- Eriksson AU, Svensson C, Hornblad A, Cheddad A, Kostromina E, Eriksson M, Norlin N, Pileggi A, Sharpe J, Georgsson F, Alanentalo T, Ahlgren U (2013) Near infrared optical projection tomography for assessments of  $\beta$ -cell mass distribution in diabetes research. *J Vis Exp* (71):e50238.
- Fernandez DC, Fogerson PM, Lazzzerini Ospri L, Thomsen MB, Layne RM, Severin D, Zhan J, Singer JH, Kirkwood A, Zhao H, Berson DM, Hattar S (2018) Light affects mood and learning through distinct retina-brain pathways. *Cell* 175:71–84 e18.
- Foster RG, Roenneberg T (2008) Human responses to the geophysical daily, annual and lunar cycles. *Curr Biol* 18:R784–R794.
- Foster RG, Peirson SN, Wulff K, Winnebeck E, Vetter C, Roenneberg T (2013) Sleep and circadian rhythm disruption in social jetlag and mental illness. *Prog Mol Biol Transl Sci* 119:325–346.
- Freedman MS, Lucas RJ, Soni B, von Schantz M, Muñoz M, David-Gray Z, Foster R (1999) Regulation of mammalian circadian behavior by non-rod, non-cone, ocular photoreceptors. *Science* 284:502–504.
- Gerfen CR, Paletzki R, Heintz N (2013) GENSAT BAC cre-recombinase driver lines to study the functional organization of cerebral cortical and basal ganglia circuits. *Neuron* 80:1368–1383.
- Haber SN (2016) Corticostriatal circuitry. *Dialogues Clin Neurosci* 18:7–21.
- Halford S, Freedman MS, Bellingham J, Inglis SL, Poopalasundaram S, Soni BG, Foster RG, Hunt DM (2001) Characterization of a novel human opsin gene with wide tissue expression and identification of embedded and flanking genes on chromosome 1q43. *Genomics* 72:203–208.
- Haltaufderhyde K, Ozdeslik RN, Wicks NL, Najera JA, Oancea E (2015) Opsin expression in human epidermal skin. *Photochem Photobiol* 91:117–123.
- Hirayama J, Miyamura N, Uchida Y, Asaoka Y, Honda R, Sawanobori K, Todo T, Yamamoto T, Sassone-Corsi P, Nishina H (2009) Common light signaling pathways controlling DNA repair and circadian clock entrainment in zebrafish. *Cell Cycle* 8:2794–2801.
- Kojima D, Mori S, Torii M, Wada A, Morishita R, Fukada Y (2011) UV-sensitive photoreceptor protein OPN5 in humans and mice. *PLoS One* 6:e26388.
- Lamb TD, Patel H, Chuah A, Natoli RC, Davies WIL, Hart NS, Collin SP, Hunt DM (2016) Evolution of vertebrate phototransduction: cascade activation. *Mol Biol Evol* 33:2064–2087.
- Lucas RJ, Hattar S, Takao M, Berson DM, Foster RG, Yau KW (2003) Diminished pupillary light reflex at high irradiances in melanopsin-knockout mice. *Science* 299:245–247.
- Matsue K, Minakawa S, Kashiwagi T, Toda K, Sato T, Shioda S, Seki T (2018) Dentate granule progenitor cell properties are rapidly altered soon after birth. *Brain Struct Funct* 223:357–369.
- Miller AM, Treloar HB, Greer CA (2010) Composition of the migratory mass during development of the olfactory nerve. *J Comp Neurol* 518:4825–4841.
- Nayak G, Zhang KX, Vemarraju S, Odaka Y, Buhr ED, Holt-Jones A, Kernodle S, Smith AN, Upton BA, D'Souza S, Zhan JJ, Diaz N, Nguyen MT, Mukherjee R, Gordon SA, Wu G, Schmidt R, Mei X, Petts NT, Batie M, et al. (2020) Adaptive thermogenesis in mice is enhanced by Opsin 3-dependent adipocyte light sensing. *Cell Rep* 30:672–686.e8.
- Neudorfer C, Maarouf M (2018) Neuroanatomical background and functional considerations for stereotactic interventions in the H fields of Forel. *Brain Struct Funct* 223:17–30.
- Nissilä J, Mänttari S, Särkioja T, Tuominen H, Takala T, Timonen M, Saarela S (2012) Encephalopsin (OPN3) protein abundance in the adult mouse brain. *J Comp Physiol A Neuroethol Sens Neural Behav Physiol* 198:833–839.
- Olinski LE, Lin EM, Oancea E (2020a) Illuminating insights into opsin 3 function in the skin. *Adv Biol Regul* 75:100668.
- Olinski LE, Tsuda AC, Kauer JA, Oancea E (2020b) Endogenous Opsin 3 (OPN3) protein expression in the adult brain using a novel OPN3-mCherry knock-in mouse model. *eNeuro* 7:ENEURO.0107-20.2020.
- Ortiz SB, Hori D, Nomura Y, Yun X, Jiang HY, Yong H, Chen J, Paek S, Pandey D, Sikka G, Bhatta A, Gillard A, Steppan J, Kim JH, Adachi H, Barodka VM, Romer L, An SS, Shimoda LA, Santhanam L, et al. (2018) Opsin 3 and 4 mediate light-induced pulmonary vasorelaxation that is potentiated by G protein-coupled receptor kinase 2 inhibition. *Am J Physiol Lung Cell Mol Physiol* 314:L93–L106.
- Panaliappan TK, Wittmann W, Jidigam VK, Mercurio S, Bertolini JA, Sghari S, Bose R, Patthey C, Nicolis SK, Gunhaga L (2018) Sox2 is required for olfactory pit formation and olfactory neurogenesis through BMP restriction and *Hes5* upregulation. *Development* 145:dev153791.



- Patthey C, Gunhaga L (2011) Specification and regionalisation of the neural plate border. *Eur J Neurosci* 34:1516–1528.
- Provencio I, Jiang G, De Grip WJ, Hayes WP, Rollag MD (1998) Melanopsin: an opsin in melanophores, brain, and eye. *Proc Natl Acad Sci USA* 95:340–345.
- Reemst K, Noctor SC, Lucassen PJ, Hol EM (2016) The indispensable roles of microglia and astrocytes during brain development. *Front Hum Neurosci* 10:566.
- Regard JB, Sato IT, Coughlin SR (2008) Anatomical profiling of G protein-coupled receptor expression. *Cell* 135:561–571.
- Reid VM, Dunn K, Young RJ, Amu J, Donovan T, Reissland N (2017) The human fetus preferentially engages with face-like visual stimuli. *Curr Biol* 27:1825–1828.e3.
- Rodier PM (1980) Chronology of neuron development: animal studies and their clinical implications. *Dev Med Child Neurol* 22:525–545.
- Roecklein KA, Rohan KJ, Duncan WC, Rollag MD, Rosenthal NE, Lipsky RH, Provencio I (2009) A missense variant (P10L) of the melanopsin (OPN4) gene in seasonal affective disorder. *J Affect Disord* 114:279–285.
- Schlosser G (2014) Early embryonic specification of vertebrate cranial placodes. *Wiley Interdiscip Rev Dev Biol* 3:349–363.
- Sghari S, Davies WIL, Gunhaga L (2020) Elucidation of cellular mechanisms that regulate the sustained contraction and relaxation of the mammalian iris. *Invest Ophthalmol Vis Sci* 61:5.
- Sharpe J, Ahlgren U, Perry P, Hill B, Ross A, Hecksher-Sørensen J, Baldock R, Davidson D (2002) Optical projection tomography as a tool for 3D microscopy and gene expression studies. *Science* 296:541–545.
- Shichida Y, Matsuyama T (2009) Evolution of opsins and phototransduction. *Philos Trans R Soc Lond B Biol Sci* 364:2881–2895.
- Sikka G, Hussmann GP, Pandey D, Cao S, Hori D, Park JT, Steppan J, Kim JH, Barodka V, Myers AC, Santhanam L, Nyhan D, Halushka MK, Koehler RC, Snyder SH, Shimoda LA, Berkowitz DE (2014) Melanopsin mediates light-dependent relaxation in blood vessels. *Proc Natl Acad Sci USA* 111:17977–17982.
- Sugihara T, Nagata T, Mason B, Koyanagi M, Terakita A (2016) Absorption characteristics of vertebrate non-visual Opsin, Opn3. *PLoS One* 11:e0161215.
- Sun L, Peräkylä J, Kovalainen A, Ogawa KH, Karhunen PJ, Hartikainen KM (2016) Human brain reacts to transcranial extracranial light. *PLoS One* 11:e0149525.
- Tarttelin EE, Bellingham J, Bibb LC, Foster RG, Hankins MW, Gregory-Evans K, Gregory-Evans CY, Wells DJ, Lucas RJ (2003a) Expression of opsin genes early in ocular development of humans and mice. *Exp Eye Res* 76:393–396.
- Tarttelin EE, Bellingham J, Hankins MW, Foster RG, Lucas RJ (2003b) Neuropsin (Opn5): a novel opsin identified in mammalian neural tissue. *FEBS Lett* 554:410–416.
- Vermeiren S, Bellefroid EJ, Desiderio S (2020) Vertebrate sensory ganglia: common and divergent features of the transcriptional programs generating their functional specialization. *Front Cell Dev Biol* 8:587699.
- Wittmann W, Schimmang T, Gunhaga L (2014) Progressive effects of N-myc deficiency on proliferation, neurogenesis, and morphogenesis in the olfactory epithelium. *Dev Neurobiol* 74:643–656.
- Wu AD, Dan W, Zhang Y, Vemmaraju S, Upton BA, Lang RA, Buhr ED, Berkowitz DE, Gallos G, Emala CW, Yim PD (2021) Opsin 3-G<sub>αs</sub> promotes airway smooth muscle relaxation modulated by G protein receptor kinase 2. *Am J Respir Cell Mol Biol* 64:59–68.
- Xue T, Do MT, Riccio A, Jiang Z, Hsieh J, Wang HC, Merbs SL, Welsbie DS, Yoshioka T, Weissgerber P, Stolz S, Flockerzi V, Freichel M, Simon MI, Clapham DE, Yau KW (2011) Melanopsin signalling in mammalian iris and retina. *Nature* 479:67–73.
- Yamanaka K, Hori Y, Minamimoto T, Yamada H, Matsumoto N, Enomoto K, Aosaki T, Graybiel AM, Kimura M (2018) Roles of centromedian parafascicular nuclei of thalamus and cholinergic interneurons in the dorsal striatum in associative learning of environmental events. *J Neural Transm (Vienna)* 125:501–513.
- Yim PD, Hyuga S, Wu AD, Dan W, Vink JY, Gallos G (2020) Activation of an endogenous opsin 3 light receptor mediates photo-relaxation of pre-contracting late gestation human uterine smooth muscle *ex vivo*. *Reprod Sci* 27:1791–1801.
- Yokoyama S (2000) Molecular evolution of vertebrate visual pigments. *Prog Retin Eye Res* 19:385–419.
- Zhang KX, D'Souza S, Upton BA, Kernodle S, Vemmaraju S, Nayak G, Gaitonde KD, Holt AL, Linne CD, Smith AN, Petts NT, Batie M, Mukherjee R, Tiwari D, Buhr ED, Van Gelder RN, Gross C, Sweeney A, Sanchez-Gurmaches J, Seeley RJ, et al. (2020) Violet-light suppression of thermogenesis by opsin 5 hypothalamic neurons. *Nature* 585:420–425.